From “source to sink” – A new perspective on the past dynamics of the Murray Canyon Group from benthic foraminiferal communities

M. Mojtahid, Elisabeth Michel, P. de Deckker

From "source to sink" - a new perspective on the past dynamics of the Murray Canyon Group from benthic foraminiferal communities

M. Mojtahid[*1,3], E. Michel[2], P. De Deckker[3]

* Corresponding author: e-mail: meryem.mojtahid@univ-angers.fr

[1] LPG-BIAF UMR-CNRS 6112, UNIV Angers, CNRS, UFR Sciences, 2 bd Lavoisier 49045, Angers Cedex 01, France

[2] Laboratoire des Sciences du Climat et de l'Environnement, LSCE/IPSL, CEA-CNRS-UVSQ, Université Paris-Saclay, l'Orme des merisiers, F-91191 Gif-sur-Yvette, France

[3] Research School of Earth Sciences, The Australian National University, Canberra, ACT 2600, Australia

Keywords

Turbidites; Last Glacial; River Murray; Bouma-like sequence; Shelf foraminifera; Bathyal foraminifera; Abyssal foraminifera

Abstract

We present fossil benthic foraminiferal assemblage data from marine sediment core SS02/06-GC2 located in the abyssal plain of the Murray Canyon Group (offshore South Australia). The sedimentological characteristics indicate the presence of turbidite deposits showing classical Bouma-like sequences, dated between ~40 and 12 cal ka BP. These results confirm the previous interpretation of the observed large deep-water holes in the abyssal area where the core was sampled as being gouged by surges of high-energy turbidity currents. The presence of good indicator taxa and unique assemblages occupying specific bathymetric depths allows the determination of the source origin of the sediments making the turbidites. Three distinct faunal groups are found: 1) mostly shelf species, 2) mostly bathyal species and 3) mostly abyssal species. In the sediment core, these groups present a quasi-systematic succession, with nearly all Bouma-like sequences starting with the dominance of bathyal species in the coarse-grained base, followed by the dominance of shallow species in the silty part, and finally with abyssal species in the clays. To explain such phenomena, turbidites triggered by mixed hyperpycnal/hypopycnal flow processes and turbidity currents during periods of river floods are considered for the first time within the Murray Canyon Group. They are mostly related to periods of increased fluvial discharges during wet phases in the Murray-Darling Basin.

1. Introduction

Submarine canyons are steep-sided valleys on continental margins and play a major role as conduits to the deep sea for sediment and organic material from the continental domain, as well as from slope and shelf (e.g. Shepard, 1972; Weaver et al., 2000; Mulder et al., 2004; Allen and Durrieu de Madron, 2009; Quattrini et al., 2015). The major mechanism of canyon erosion is believed to be turbidity currents (e.g. Bouma et al., 1985; Azpiroz-Zabala et al., 2017). These dense sediment-laden currents flow downslope when an unstable upper slope mass of sediment fails under the influence of climatic factors (e.g. sea-level changes, high river discharge, marine currents, coastal storms) and non-climatic factors (e.g. earthquakes, tsunamis, volcanic eruption, storm surges, release of gas hydrates) (e.g. Garidel-Thoron et al., 2004; Piper and Normark, 2009; Bernhardt et al., 2016). These phenomena are generally identified in marine sediment cores as Bouma-like turbiditic sequences (Bouma et al., 1962). Because of rapid organic material transport down slope, turbidity currents funneled through canyons very likely enhance marine biodiversity, especially in the deep-sea (e.g. McClain and Barry, 2010; Fernandez-Arcaya et al., 2017), and constitute “accelerators” for carbon sequestration (e.g. Schlünz and Schneider, 2000; Galy et al., 2007). Much progress has been made in describing the morphology of submarine canyons at high spatial resolution, mainly because of the considerable advances in imaging using the latest generation of multibeam technology (e.g. Hill et al., 2005; Lastras et al., 2009; Mountjoy et al., 2009; Paull et al., 2010). An important gap remains, however, in our understanding of the processes that shape these submarine canyon systems, and how they respond to climatic and non-climatic influences. In particular, the source and the triggering origin of turbidity currents are still a matter of

63 debate (e.g. Piper and Normark, 2009; Covault and Graham, 2010). One way to address
64 this issue is to investigate the processes that control fluvial/canyon connections recorded
65 in marine sediment cores during the Quaternary geological period modulated by
66 glacial/interglacial cycles under contrasting sea-level stands and climatic conditions (e.g.
67 Lombo Tombo et al., 2015; Mauffrey et al., 2015).
68 Fossil benthic foraminiferal faunas preserved in deep-sea Quaternary sediment cores at
69 the outlet of canyons are good candidates to record changes in depositional environments
70 and palaeo-water depths. Foraminifera have previously been used to assist in identifying
71 and determining the provenance of Late Quaternary turbidites (e.g. Strachan et al., 2016;
72 Hayward et al., 2004, 2019). In order to assign a depth range to a species in the fossil
73 record, we often rely on studies of modern settings where bathymetry and associated
74 environmental parameters are accurately measured. These bathymetric intervals are then
75 applied on a generic level to the fossil record (e.g. Schröder-Adams et al., 2008). When
76 determining palaeo-depths, it is fundamental to distinguish autochthonous from
77 transported (allochthonous) faunal taxa since gravity processes frequently transport
78 benthic foraminifera from the inner continental shelf to the abyssal plain together with
79 sediment particles. The foraminifera tests may suffer abrasion or dissolution when
80 transported and deposited close to or below the Calcite Compensation Depth (CCD).
81 Here, we investigate the past (~40 to 12 ka) dynamics of one of the canyons in the
82 Murray Canyon Group offshore Kangaroo Island (South Australia) using benthic
83 foraminiferal assemblages from a 5,078 m-water depth sediment core (SS02/06-GC2)
84 (Fig. 1). The existence of this major canyon system was first recognized by Sprigg (1948)
85 and, since then, several studies have been published, mainly after the two AUSCAN

86 cruises in 2003 and 2006 (e.g. Gingele et al., 2004; Hill and De Deckker, 2004; Gingele
87 and De Deckker, 2005; Hill et al., 2005; Calvo et al., 2007; Gingele et al., 2007; Moros et
88 al., 2009; Schmidt et al., 2010; De Deckker et al., 2012; Lopes dos Santos et al., 2012,
89 2013; Bayon et al., 2017, 2020). Most of these studies tackled the recent morpho-
90 bathymetric features and sedimentary processes of the canyons or investigated Late
91 Quaternary environments using sediment cores away from the main turbidity pathways.
92 Yet, the origin of the canyon system itself is still largely unknown. Some canyons are
93 thought to be related to ancient courses of the River Murray and could have provided a
94 pathway during low sea levels to bring sediments from the River directly to the abyssal
95 area (Gingele et al., 2004). These sediments flowing into the abyss for millions of years
96 carry geochemical and palaeontological signatures of past climatic and environmental
97 conditions. Hill and De Deckker (2004) and Hill et al. (2005) described the presence of
98 large deep-water holes in the abyssal area, spaced about 5 km apart and up to several
99 hundred meters deep (Fig. 1), that were interpreted as probably being gouged by surges
100 of high-energy turbidity currents, which such steep canyons could generate. Core
101 SS02/06-GC2 is located in one of these topographic depressions at one of the outlet
102 channels of the larger and steeper canyons of the Murray Canyon Group (Fig. 1).
103 This study uses benthic foraminifera and sediment characteristics of the core to
104 distinguish between displaced downslope and in-situ hemipelagic sediments, with the aim
105 of identifying the provenance of the turbidites of Late Quaternary age. When comparing
106 the palaeoecological interpretations obtained from the characterization of benthic
107 foraminiferal communities with climatic and continental proxies from the existing
108 literature in the area, we further aim at reconstructing the sedimentary imprints of the

interplay between sea level and climatic changes, and their relative importance for triggering turbidity currents.

1. Study area

Gravity core SS0/06-GC2 (255 cm long; 37°07.980' S; 136°29.735' E) was sampled in March 2006 during the "AUSCAN 2006 and PALAEO-MURRAYS" cruise onboard the RV *Southern Surveyor* south of the upper Sprigg Canyon at the depth of 5,078 m (Fig. 1). The Murray Canyon Group, located in the southeastern continental margin of Australia (Fig. 1a; b), are amongst the biggest canyon systems in the world (~5 km drop with up to 2 km high canyon walls). The continental shelf bordering the Murray Canyon Group is known as the "carbonate factory" because it is the largest region of cool-water carbonate sediment deposition in the modern world (e.g. James et al., 1994; James and Bone, 2011; James et al., 2013). For this reason, seawater in this region is supersaturated with respect to both aragonite and calcite at least down to depths of 1,000 m (James et al., 2005). Cores from the southern Indian Ocean south of Australia show that the CCD lies at 4,800-4,900 m (Mallet and Heezen, 1977; Belyaeva and Burmistrova, 1985). This deep CCD explains the abyssal plain seabed sediments being mostly foraminifer-nannofossil ooze (Feary et al., 1993; Dutkiewicz et al., 2015), and the overall good preservation of foraminiferal tests in our sediment core.

The Murray Canyon Group is located off the Murray-Darling River mouth (referred to in this manuscript as the River Murray mouth for simplicity) (Gingele and De Deckker, 2005), which is Australia's largest exorheic river system (Bourman et al., 2016) (Fig. 1a). The modern discharge at the Murray mouth is highly dependent on rainfall intensity in

132 the Murray-Darling Basin (e.g. Grafton et al., 2014). An average of 5,088.10^6 m^3 yr^{-1}
133 (~160 m^3 s^{-1}) was recorded during a relatively wet period on the continent (1980–2001)
134 while during the more recent dry years (2002-2010), flows at the Murray Mouth dropped
135 by about 96 % reaching an average of 190.10^6 m^3 yr^{-1} (~6 m^3 s^{-1}) (Grafton et al., 2014).
136 Because the Murray mouth is presently ~200 km away from the canyons, little
137 terrigenous material from the Murray Darling Basin reaches the study area and sediments
138 consist mainly of pelagic carbonate particles and aeolian dust (e.g. Bayon et al., 2017,
139 2020). There is however evidence of some fluvial clays reaching the core sites during the
140 last 6 ka, after the stabilization of sea level (Gingele et al., 2004). By using a multi-tracer
141 approach (^{210}Pb and ^{230}Th) on interface sediments from the Murray canyons (350 - 2500
142 m water depths), the study of Schmidt et al. (2010) shows the presence of freshly
143 deposited carbonate particles. This finding supports the occurrence of recent, significant
144 advection of marine sediments, mostly from the shelf, within these canyons.
145 Because the entrance of the canyons start at around the 120 m isobath (Figure 1a, b), a
146 larger fluvial sedimentary input to the deep-sea was present during minimum sea-level
147 stands (during oxygen isotope stages 2, 4 and 6) as the Murray mouth was probably at the
148 present shelf edge and almost directly connected to the canyons (Gingele et al., 2004; Hill
149 et al., 2009). The well-defined 'glacial' channels (= formed during periods of low sea
150 level) on the adjacent continental shelf show that the Murray River traversed the shelf
151 from the location of its current mouth towards the submarine canyons south of Kangaroo
152 Island (Sprigg, 1948; Hill et al., 2005, 2009).
153 In terms of water masses, the Circumpolar Deep Water (CPDW) (Emery and Meincke,
154 1986) derived from the Antarctic Circumpolar Current and the Antarctic Bottom Waters

(AABW) are the main deep water masses occurring from bottom to about ~1200 m water depth (Fig. 1c). From ~1200 m to 850 m, the Antarctic Intermediate Water (AAIW) is present and from ~850 to 450 m depth, the Sub-Antarctic Mode Water (SAMW) is dominant (Passlow et al., 1997) (Fig. 1c). Surface waters (250 – 0 m) are mainly represented by the Subtropical Surface Water (STSW) (Richardson et al., 2019) (Figure 1a; c). These surface waters are affected by the Leeuwin Current (LC), a winter stream of warm, relatively low-salinity, tropical, surface water. The LC hydrographic properties are well defined: Tropical Surface Water (TSW) from northwestern Australia and South Indian Central Water (SICW) from the West Australian Current mix and flow south and then east along the southern margin (Cresswell and Peterson, 1993; Woo and Pattiaratchi, 2008; Richardson et al., 2019) (Fig. 1a). Today and during the Holocene, the LC is/was most effective at reaching 135-140°E during the austral winter, during La Niña phases, that affect the region (De Deckker et al., 2012; Perner et al., 2018). During the last glacial period, the LC was overall absent or weaker in the study area (De Deckker et al., 2012). The Flinders Undercurrent also passes over the Murray Canyon Group and flows west along the continental slope of southern Australia (cf. Middleton and Bye (2007) for further details). The LC overrides the Flinders Undercurrent when present.

2. Material and methods

Radiocarbon dating was determined by accelerator mass spectrometry on mono-specific samples of the planktonic foraminiferal species *Globorotalia inflata* and *Orbulina universa*, except for one sediment sample (212 cm) for which we used a mixture of the two species (Table 1). A minimum of 7 mg per sample was extracted from the >150 μm

size fraction in seven sediment samples (Table 1). Only the muddy intervals, theoretically representing the hemipelagic sedimentation, were selected for dating (Fig. 2). Radiocarbon dating was performed by UMS-ARTEMIS (Pelletron 3MV) AMS facilities (CNRS-CEA Saclay, France), following the standard procedure described by Tisnérat-Laborde et al. (2001). For the three sediment levels where two ^{14}C dates were obtained (23-24 cm, 45-46 cm et 160-161 cm; Table 1), we calculated the average ^{14}C age and we combined the errors using propagation of uncertainty. Conversion into calendar years was obtained with Calib7.1.0 software and the "SHCal13" calibration curve (Hogg et al., 2013; Reimer et al., 2013) after applying a −367 ± 167 year reservoir correction (average value from four nearest locations from the global data base in http://www.calib.qub.ac.uk/marine).

Using visual observation and high-resolution photographs (Fig. 2), we performed a detailed and rigorous visual description of the studied core in terms of lithology, sedimentary structures, bioturbation features and colour (Fig. 2). All these observations were compiled in the form of a sedimentological log and a descriptive curve of the three main grain size fractions presented in Fig. 2.

The core was sub-sampled at different sediment layers and were each one cm thick, guided by the various sedimentological features (Fig. 2). The collected samples were washed over sieves of 150 μm openings, dried and split with an Otto microsplitter. Whole splits were counted until a minimum of 200 tests of benthic foraminifera was obtained. Foraminifera were then picked under the binocular. The benthic foraminiferal faunas were analysed for different sediment layers following the various sedimentological features (Fig. 2). For each subsample, a known volume of sediment was

processed for foraminiferal analysis, wet-weighed, dried and re-weighed to obtain dry weight. Benthic foraminiferal species ranging from estuarine, upper shelf to abyssal faunas were identified using reference taxonomic studies in the area (Hayward et al., 1999, 2010; Debenay, 2012). In order to help with taxonomical identification, Scanning Electron Microscope (SEM) photographs were obtained at the Centre for Advanced Microscopy (Australian National University, Canberra) using the Zeiss UltraPlus analytical FESEM after Gold coating the specimens in an EMITECH EMITECH K550X coater (Plates 1 to 4).

Diversity (Shannon H) index and Principal Component Analysis (PCA) was calculated using the software PAST (PAleontological STatistics; Version 3.25; Hammer et al., 2001). Input for the PCA consisted of species' relative abundance data (correlation matrix). Only taxa occurring with ≥5% in at least one sample were retained in these statistical analyses.

3. Results

3.1. Lithology and grain size

Core SS02/06-GC2 is characterized by a succession of sediment layers of variable colours spanning from light to dark olive-grey sediments from 255 to 95 cm depth to light brownish grey sediments in the top 95 cm (using a Munsell colour chart codes in Fig. 2). Every colour change is accompanied in most cases by a change in particle size (Fig. 2). The range of particle sizes is large, going from clays to silts to coarse sands, with the sandy and silty levels being usually rich in shell debris (Fig. 2). Several erosional

224 contacts are also observed along the core. All these lithological features are indicative of
225 a dynamic and likely discontinuous sedimentation due to high-energy reworking and
226 transport processes, such as those characterizing submarine canyon turbidity deposits (e.g.
227 Mulder et al., 2012; Lombo Tombo et al., 2015). These turbidites are mostly
228 characterized by a normal grading, going from coarse sand at the base into finer sand silt
229 and clay upward, and often, an erosional base is present (Fig. 2). The unavailability of
230 high resolution X-ray images prevent us from a more detailed description of the different
231 lithofacies, and especially from identifying sedimentary structures such as linear/crossed
232 laminations that could help us discriminating between the various turbidite sequences (e.g.
233 Mulder et al., 2003; Shanmugam, 2018).
234 Because of the presence of turbidite deposits, we decided not to build an age model for
235 this study and only use the obtained ^{14}C dates to give a general chronological framework.
236 The results show that core SS02/06-GC2 covers a time-period from ~40 to 12 cal ka BP,
237 with a discontinuous sedimentation. Caution is required regarding ^{14}C ages, as turbidites
238 seem to have been deposited only at four specific time-periods: 1) At ~40-35 cal ka BP
239 (between ~255 cm and 181 cm sediment depth), 2) at ~32 cal ka BP (from ~181 cm to
240 157 cm), 3) at ~21 cal ka BP, (from ~157 cm to 122 cm), and 4) at ~12.8 cal ka BP (the
241 upper ~122 cm) (Figs. 2 and 5). Since there are no ^{14}C ages above 23 cm sediment depth,
242 perhaps a part of these sediments may have been deposited later during the Holocene.
243

244 ***3.2. Foraminiferal analyses***

245 A total number of 294 benthic foraminiferal species were determined in core SS02/06-
246 GC02, among which 33 are dominant and show relative abundances ≥5% in at least one

247 sample. In order to facilitate examination of the large dataset obtained (Dataset S1) and to
248 extract the main faunal ecological groups, a PCA was performed based on the percentage
249 data of these dominant taxa (Fig. 3a). Axes 1 and 2 account respectively for 20.86% and
250 16.33% of the total variance of the dataset. The PCA separates the faunal assemblages
251 into three main species groups with rather similar bathymetric/ecological characteristics
252 (Fig. 3b):
253 Group 1 is composed of *Rosalina bradyi/globularis*, *Miliolinella subrotundata*,
254 *Sphaeroidina bulloides*, *Elphidium excavatum, Elphidium crispum*, *Gavelinopsis*
255 *praegeri*, *Rosalina anomala*, *Nonion pacificum/Haynesina depressula*, *Spirillina* sp., and
256 *Bolivina earlandi*. Most of these species are outer estuarine/inner continental shelf
257 species (e.g. Hayward et al., 1999, 2010; Debenay, 2012; Mojtahid et al., 2016) (Fig. 3b).
258 *Nonion pacificum* and *H. depressula* are lumped together because the taxonomic
259 differentiation between these two morphologically similar species has been problematic.
260 Especially, we could not systematically observe the star-shaped umbilicus characteristic
261 of *H. depressula*, probably because abrasion during transport from shallow depths
262 towards the abyssal area may have altered the tests.
263 Group 2 is composed of *Uvigerina mediterranea, Spiroplectinella proxispira, Cibicides*
264 *refulgens, Cibicides variabilis, Cibicidoides pachyderma, Cibicidoides dispars* s.l.*,*
265 *Cibicides lobatulus, Globocassidulina subglobosa, Quinqueloculina auberiana, Trifarina*
266 *angulosa,* and *Notorotalia clathrata.* Most of these species have in common a bathyal
267 depth habitat according to their modern distribution and most extend onto mid to outer
268 shelf as well (e.g. Li et al., 1996; Hayward et al., 1999, 2010; Mojtahid et al., 2010;
269 Debenay, 2012) (Fig. 3b).

Group 3 is composed of *Epistominella exigua/vitrea, Cibicidoides wuellerstorfi, Melonis affinis/barleeanus, Nuttalides umbonifera, Pullenia bulloides, Oridorsalis umbonatus, Oridorsalis tenerus, Oolina* spp.*, Gyroidina orbicularis, Fursenkoina complanata, Cibicidoides robertsonianus,* and *Uvigerina peregrina* s.l. Although these species have a large bathymetric range, they all inhabit lower bathyal to abyssal depths (e.g. Hayward et al., 1999, 2010; Mojtahid et al., 2010; Debenay, 2012) (Fig. 3b).

All groups are present throughout the record, but each of them dominates specific sediment intervals (Figs 4; 5d):

Group 1 (mostly shelf faunas) is dominant at 255-220 cm, 188-183 cm, 170-169 cm, 92-91 cm, 61-59 cm, 31-30 cm and 6-2 cm sediment depths (cf. light grey bands in Fig. 4). Except for the sandy 255-220 cm sediment interval, this group dominates the silty levels that are characterized by intermediate total absolute densities of foraminiferal faunas (164±183 g/dry sediment) and the highest Shannon index (3.56±0.16) and total species number (69±16) (Fig. 4).

Group 2 (mostly bathyal faunas) is dominant at 199-190 cm, 178-179 cm*, 118-119 cm*, 125-99 cm, 95-94 cm*, 64- 63 cm, and 34-33 cm sediment depths (cf. dark grey bands in Fig. 4). This group dominates the sandy and coarse sandy levels that are characterized by maximum total absolute densities of foraminiferal faunas (791±483 g/dry sediment) and intermediate Shannon index (3.45±0.16) and total species number (55±9) (Fig. 4). The samples indicated by an asterisk were investigated only qualitatively because of some sediment loss.

292 Group 3 (mostly abyssal faunas) is dominant at 213-204 cm, 184-183 cm, 161-130 cm,
293 86-68 cm, 56-38 cm, 24-14 cm, and 1-0 cm sediment depths (cf. white bands in Fig. 4).
294 This group dominates the clayey levels that are characterized by minimum total absolute
295 densities of foraminiferal faunas (26±9 g/dry sediment) and minimum Shannon index
296 (3.14±0.44) and total species number (47±16) (Fig. 4).
297
298 **4. Discussion**
299 *4.1. Succession of sediment deposits in the abyssal plain of the Murray Canyon*
300 *Group*
301 The studied abyssal site is characterized by obviously very dynamic and discontinuous
302 sedimentation, indicated by clear changes in sediments colours, several erosional
303 surfaces and a highly fluctuating grain size distribution spanning from coarse sands to
304 clays (Fig. 5a-b). This is further corroborated by the ^{14}C dates showing short time
305 periods of large sediment deposits (e.g. ~40-35 ka cal BP and ~12.8 ka cal BP),
306 interrupted by periods of lower sedimentation rates and probably lack of sedimentation
307 (Fig. 2). All these sedimentary features point to a succession of turbidite deposits (Fig.
308 5a-b), corroborating, therefore, the morphobathymetric map interpretation of the large
309 deep-water holes in the abyssal area (Fig. 1b) being gouged by surges of turbidity
310 currents (Hill and De Deckker, 2004; Hill et al., 2005). These turbidites are characterized
311 by a normal grading (Fig. 5b), going from coarse sand at the base into finer sand silt and
312 clay upward (e.g. Bouma et al., 1962; Middleton and Hampton, 1973; Walker, 1976;
313 Lowe, 1982; Shanmugam, 1997) (Fig. 5e). Regarding these sedimentological
314 characteristics, the turbidite sequence deposits can be described as distal (i.e. absence of

315 pebbles ; Walker, 1976), “classical” Bouma-like sequences (Figure 5e). In core SS02/06-
316 GC2, we do not always observe an entire Bouma sequence; sometimes it seems to be
317 truncated either of its higher layers (e.g. 120-115 cm sediment depth) or of its lower
318 layers (e.g. 150-125 cm sediment depth) (Fig. 5b). For simplicity, we defined seven
319 Bouma-like sequences (Bs1 to Bs7), without considering the “small” turbidity events, or
320 the truncated sequences (Fig. 5b).
321 Bouma et al. (1962) associated the vertical evolution of the terms, from “T_a” to “T_e” (Fig.
322 5e), with over time the evolution of the transport capacity and the speed of the turbidity
323 current. Indeed, the energy (bed shear stress) is decreasing upwards as the current passes
324 by, and this is also manifested in the normal grading of the bed – coarser at the base,
325 finer at the top (e.g. Zavala et al., 2011). Although evidence of reworking and transport
326 is present in all samples, it is in the silty and sandy layers of the turbidites that this is
327 most obvious with the high abundance of shallow (e.g. *Rosalina* spp., *Elphidium* spp.)
328 and bathyal benthic species (e.g. *U. mediterranea*, *C. refulgens*) (Figs. 4 and 5d). This
329 feature is common in other turbidity systems (e.g. Zaragosi et al., 2006; Lombo Tombo
330 et al., 2015). Because it contains few shallow and bathyal benthic foraminifera, some of
331 the clay might have been introduced into the area by the turbidity current and/or by
332 river-generated plumes, but since it contains mostly abyssal benthic species (e.g.
333 *Epistominella* spp., *C. wuellerstorfi*), the clay layer more likely represents the constant
334 slow rain of mud onto the ocean floor (Figs. 4 and 5d).
335
336 *4.2. Source of the abyssal turbidite deposits inferred from benthic foraminiferal*
337 *communities*

338 According to Middleton and Hampton (1973), classical turbidity sequences such as the
339 one we observed here, result from low-concentration turbidity currents that are either
340 initiated by a river in flood or slump/slide processes from the upper slope. In core
341 SS02/06-GC2, the presence of very shallow inner shelf species (e.g. *Rosalina* spp., *E.*
342 *crispum*) and some outer estuarine species (*E. excavatum* and most probably *H.*
343 *depressula*) (Hayward et al., 2010, 1999; Debenay, 2012) (PCA group 1; Fig. 3) mainly
344 in the silty layers of the turbidite deposits (Figs. 4 and 5), indicate an inner shelf-related
345 source, most likely nearby the Murray mouth. Additionally, within PCA group 1, we
346 observed that individuals are overall small-sized belonging mostly to flat-shaped
347 foraminiferal species (e.g. *Elphidium* spp., *Rosalina* spp., *G. praegeri*), some of which
348 are known for their epibenthic/epiphytic habitats (e.g. *Rosalina* spp.). All these criteria
349 make these species particularly prone to transport, in suspension or attached to floating
350 sea grass or algae (Jorissen and Whittling, 1999; Murray, 2006), by currents and/or river
351 plumes during periods of high river runoff (e.g. Duros et al., 2012; Garcia et al., 2013;
352 Mojtahid et al., 2013; Durand et al., 2018). Therefore, our foraminiferal observations
353 seem to argue in favour of a river in flood origin, at least for the silty layers. In that case,
354 one of the most documented mechanisms of implementation could be the presence of
355 hyperpycnal currents (e.g. Mulder et al., 1997). Using experimental models and in-situ
356 measurements, the particulate concentration threshold necessary to generate a
357 hyperpycnal flow can be lowered from the initial value of 35-40 kg m^{-3} (e.g. Mulder et
358 al., 1997) to 5 kg m^{-3} because of concentration phenomena increasing the flow density
359 (such as by flocculation, convective instability and local hydrodynamic conditions) (e.g.
360 Parsons et al., 2001; Felix et al., 2005). As a result, about 80% of rivers worldwide can

361 engender hyperpycnal flows in the marine environment, with a frequency of less than
362 one per century (e.g. Mulder and Syvitski, 1995; Mulder et al., 2003; Wright and
363 Friedrichs, 2006). Accordingly, and despite its modern relatively low freshwater
364 discharge (6 – 160 m^3 s^{-1}; Grafton et al., 2014), the River Murray could potentially
365 produce hyperpycnal flows, at least during periods of low sea-level in the past and/or
366 periods of high river runoff.
367 Using the modern bathymetric range of each of the main benthic foraminiferal species
368 present in our core (Hayward et al., 1999, 2010; Debenay, 2012) (Dataset S1), we can
369 deduce the source origin of sediments reaching the abyssal area. In our samples, a quasi-
370 systematic succession in foraminiferal ecological PCA groups stands out for each of the
371 defined Bouma-like sequences (Fig. 5d): nearly all sequences start with the dominance
372 of bathyal species in the coarse-grained base, followed by the dominance of shallow
373 species in the silty part, and finally with abyssal species in the clays (Fig. 5d). Apart
374 from the clay layer that represents mostly the natural hemipelagic background in the
375 abyssal area, the bathyal/shallow allochthonous species succession clearly indicates two
376 different sources of transported sediments for each recorded turbidity event (i.e. one
377 Bouma-like sequence). Because there is no reason why foraminiferal species from two
378 different ecological groups follow the grain size downgrading within a turbidity current,
379 our findings clearly question a process involving a single hyperpycnal flow as we
380 previously hypothesized.
381 An alternative scenario is presented in the study of Mulder et al. (1997). According to
382 these authors, hypopycnal and mesopycnal plumes can be produced in addition to

383 hyperpycnal flows and/or turbidity currents during river floods (Fig. 6). As such, we
384 hypothesize the following scenario:
385 (1) the high sedimentation rate at the river mouth and into the adjacent ocean and
386 increased particulate load during river flood events can create high instability of the
387 upper slope at the "plunge point". This might trigger hyperpycnal flows or turbidity
388 currents when high sediment load creates shallow failures of the upper slope sediments
389 through excess pore pressure (see review in Shanmugam, 2018). In both cases, coarse
390 grained materials can be dragged at the base as bedload by shear forces, therefore
391 transporting bathyal species down to the abyssal plain. This might explain their
392 dominance in the sandy base of our Bouma-like sequences (Fig. 6b).
393 (2) meanwhile, hyperpycnal and mesopycnal plumes may have formed from the same
394 river flood event, carrying silts and clays in suspension to the abyssal plain. Shallow-
395 water benthic species with a large fraction of epiphytes/epibenthics (e.g. *Rosalina* spp.,
396 *G. praegeri*; Fig. 4) can be transported in suspension by the plumes and eventually be
397 deposited at the study site by hemipelagic sedimentation. Because this mode of
398 sedimentation is slower in time relatively to the bed load transport, the decaying silts
399 with a high proportion of shallow-water species are deposited on top of the sandy base.
400 It its however difficult to separate the silty fraction originating from the turbulent flow,
401 as strictly defined for the Bouma sequence, from that cascading from the hypopycnal
402 and mesopycnal plumes. This might explain the non-exclusive presence of either of the
403 two ecological groups in the sandy and silty layers of the turbidity deposit despite their
404 respective dominance (Fig. 6b).

405 (3) the drastic decrease in foraminiferal absolute densities and the dominance of abyssal
406 benthic species (e.g. *Epistominella* spp., *C. wuellerstorfi*) in the clayey layers of the
407 Bouma-like sequences indicate a decline and/or cessation of the turbidity current. As
408 such, the clay deposit more likely represents the constant, slow 'rain' of mud over the
409 ocean floor to which the abyssal oligotrophic species are usually adapted (Figs. 4 and
410 5d). Still, the presence of few shallow and bathyal benthic species in these muddy layers
411 might indicate that some of the clays have been transported in suspension after storms
412 for instance, by resuspension from the hypopycnal flow, and/or by a low-density current
413 as defined by Middleton and Hampton (1973) (Fig. 5e).
414
415 *4.3. Linking abyssal turbidite deposits to the climate of south Australia*
416 Based on the ^{14}C dated clayey layers, core SS2/06-GC2 covers a time-period
417 spanning from approximately 40 to 12 cal ka BP (Fig. 2). This encompasses part of the
418 last glacial period and the last deglaciation. At 40 cal ka BP, the relative sea-level (RSL)
419 was lower than today by ~-60 m and continued its falling until reaching ~-130 m at the
420 last glacial maximum (LGM) around 21 cal ka BP, followed by a rapid rise to reach ~-60
421 m at ~12 cal ka BP (Waelbroeck et al., 2002; Lambeck et al., 2014). Although it is widely
422 accepted that eustatic sea-level is a key factor controlling turbidite activity in most
423 submarine canyon systems by altering the location of sediment deposition relative to the
424 shelf edge (e.g. Lebreiro et al., 2009; Henrich et al., 2010; Pierau et al., 2010; Lombo
425 Tombo et al., 2015), it is insufficient to explain alone the timing and intensity of turbidite
426 deposits at our core location. Indeed, the largest turbidite deposits in core SS2/06-GC2
427 did not take place at the LGM when the maximum of the RSL fall was reached, but

428 occurred around ~40-35 cal ka BP (Bs1 and Bs2), ~32 cal ka BP (the early part of Bs3),
429 and ~12.8 cal ka BP (Bs4, Bs5, Bs6) (Figure 6b). Furthermore, at ~12.8 cal ka BP and
430 ~40 cal ka BP, sea-level was lower than today by ~ -60 m (Lambeck et al., 2014), and
431 therefore the palaeoshoreline was about halfway from its modern position (e.g. Gingele et
432 al., 2007), meaning that the River Murray mouth was most likely disconnected from the
433 canyon head most of the record. Furthermore, the similar foraminiferal successions in the
434 pre-Holocene turbidite sequences compared the older turbidite deposits (Fig. 5b),
435 strongly points to a common main triggering process, being rather independent from the
436 RSL. As hypothesized in our model (Fig. 6), our turbidite deposits are most likely
437 initiated by enhanced fluvial discharges.
438 A strong link exists between the intensity of fluvial sediment discharge to the Murray
439 Canyon Group and climate of SE Australia (e.g. Gingele et al., 2004, 2007; Page et al.,
440 2009; Petherick et al., 2013; Bayon et al., 2017). Considering the limitations of ^{14}C dating
441 in such dynamic sedimentary setting, the timing of large turbidite deposits in our study
442 site seems to be remarkably consistent with palaeoclimatic evidence of overall humid
443 climate on the continent:
444 *The pre-LGM*: On land, studies report significant fluvial activity in the Murray
445 Darling basin (e.g. ~30-18 ka; Petherick et al., 2013) together with higher lake levels (e.g.
446 ~55-25 ka; Page et al., 2009). The more recent study of Bayon et al. (2017) using
447 neodymium isotopes from a marine sediment core, close to our study site, further states a
448 strong link between episodes of massive iceberg discharges in the Northern Hemisphere
449 (NH) (i.e. Heinrich stadials - HS) during the last glacial period and the intensity of River
450 Murray discharges into the ocean. Such link is explained by the fact that these NH

451 cooling events were accompanied by pronounced southward migrations of the
452 Intertropical Convergence Zone (ITCZ) leading to increased monsoon rainfall as far
453 south as about 32°S (e.g. Wang, 2000; Kanner et al., 2012; Bayon et al., 2017). In our
454 core, and albeit the uncertainties of ^{14}C dating, it is interesting to note that the oldest
455 turbidite deposits around 40-35 cal ka BP (Bs1 and Bs2), and ~32 cal ka BP (the first part
456 of Bs3) seem to coincide with Heinrich stadial 4 (HS4 ~40-38 cal ka BP; Wendt et al.,
457 2019) and Heinrich stadial 3 (HS3 ~32-29 cal ka BP; Turney et al., 2016) respectively,
458 which seems therefore coherent with the conclusions of Bayon et al. (2017).

459 *The LGM:* the predominant opinion in the literature is that conditions during the
460 LGM in SE Australia (21 ± 3 cal ka BP, Reeves et al., 2013) were cold and arid (e.g.
461 Williams et al., 2006; Page et al., 2009), although some of the fluvial and lake records
462 from the Murray Darling Basin (e.g. Mueller et al., 2018) indicate the opposite. In the
463 ocean, Gingele and De Deckker (2005) report an increase in dust input from the central
464 desert areas to the Murray canyons, which they interpreted as increased aridity in the
465 Murray-Darling Basin. In our study core, the turbiditic activity seem to be low at ~21 cal
466 ka BP, as indicated by what seems to be a truncated/incomplete sequences of Bouma (the
467 upper part of Bs3; Figure 5b), although parts of turbidite deposits can be removed where
468 strong bottom currents may have prevented deposition (e.g. Stow and Smillie, 2020). The
469 larger presence of the oligotrophic species *O. umbonatus* and *O. tenerus* in the clayey
470 layers during the LGM (~157 - 122 cm; Fig. 4) compared to the other time-intervals
471 might in fact argue in favour of low fluvial nutrient input. Therefore, and being cautious
472 regarding the timing of our deposits, our finding seems to indicate decreased discharges

of the River Murray during the LGM, in connection with overall dry climate on the continent.

The pre-Holocene: Higher proportions of fluvial illite in Murray Canyon sediments between 13.5 and 11.5 ka is coherent with a general increase in Murray River discharge and more humid conditions in the catchment area (Gingele et al., 2004, 2007). Nash et al. (2018) who studied sediment cores from the River Murray paleochannels on the Lacepede shelf show a very high sediment accumulation within these ancient channels under estuarine conditions, coinciding with the drainage of meltwater pulses at the end of the last deglaciation. If it is not a matter of preservation, the concomitance between the drainage of meltwaters and wetter conditions on the continent could explain the larger number of turbidite deposits at ~12.8 cal ka BP compared to older ages. Also, we can't discard the role of strong continental shelf currents and waves in transporting sediments to the upper slope as it is the case today (Li et al., 2009). It very likely that shelf currents and waves might have started moving sediments from the recently submerged mid-inner shelf along and out to the canyon head and helped accentuating the upper slope instability at the plunge point that we hypothesized in our model (Fig. 6). Similar processes have been hypothesized to explain the large turbidite deposits during the early Holocene in the Eel fan (offshore northern California) in connection to Eel River flooding events (Paull et al., 2014). Because the Leeuwin Current is a very shallow current (flowing in the upper ~80 m of the water column when strong and the upper ~50 m when weak; Perner et al., 2018) and because it was overall absent or weak in the study area during the last glacial period and most of the deglaciation (De Deckker et al., 2012), we can't assume with high confidence that this current itself was capable of transporting

496 sediments from the shelf to the canyon head at the end of the last deglaciation.

497

498 **5. Conclusions**

499 The sedimentary and foraminiferal characteristics of core SS0/06-GC02 indicate a
500 succession of turbidites, deposited between ~40 and 12 cal ka BP. We described each of
501 the turbidite deposits as distal, "classical" Bouma-like sequences. Unsurprisingly, it is in
502 the sandy and silty layers of the turbidites that evidence of reworking and transport is
503 most found with the dominance of shallow (e.g. *Rosalina* spp.) and bathyal benthic
504 foraminiferal species (e.g. *U. mediterranea*). The presence of outer estuarine/upper inner
505 shelf species (e.g. *Rosalina* spp., *Elphidium excavatum*) argues in favour of a river in
506 flood origin causing the involved transport processes.
507 Using the modern bathymetric range of each of the main benthic species present in the
508 core, we determined the source origin of sediments arriving to the abyssal area. We find a
509 quasi-systematic succession in the three ecological PCA groups for each of the defined
510 Bouma-like sequences: nearly all sequences start with the dominance of bathyal species
511 in the coarse-grained base, followed by the dominance of shallow species in the silty
512 portion, and finally with abyssal species in the clays. Our findings clearly question a
513 process involving a single hyperpycnal flow. We hypothesize a mixed process involving:
514 i) hypopycnal and mesopycnal plumes transporting shallow water benthic species with a
515 large fraction of flat-shaped epibenthic species in suspension, and ii) hyperpycnal flow
516 and/or turbidity current when the upper slope is destabilized under fluvial sediment load,
517 dragging coarse grained material at the base transporting bathyal species to the abyssal
518 plain.

519 The largest turbidite deposits in core SS2/06-GC2 did not take place during the LGM
520 when the maximum of the RSL fall was reached, but occurred around 40-35 cal ka BP,
521 32 cal ka BP, and 12.8 cal ka BP. We hypothesize a strong link between the intensity of
522 fluvial sediment discharge to the Murray Canyon Group and climate of SE Australia, but
523 the core chronological control prevents us from being more certain of this hypothesis.
524

525 **Acknowledgements**

526 We are grateful to The Australian National Marine Facility for granting time on the RV
527 *Southern Surveyor* to collect the core and obtaining additional bathymetry data processed
528 by P. J. Hill and Michele Spinoccia. Don Mackenzie of CSIRO facilitated the collection
529 of the core and Geoscience Australia loaned the gravity corer. We are thankful to the
530 French ^{14}C AMS facility ARTEMIS for chemical preparation and measurements of the
531 ^{14}C samples. The data are available online as supplementary material and/or by
532 contacting the first author (e-mail: meryem.mojtahid@univ-angers.fr). We are very
533 grateful to Maria Pia Nardelli for scientific discussions, and to the two reviewers Bruce
534 Hayward and Maria-Angela Bassetti for their thorough reviews that significantly helped
535 improve the manuscript.
536

537 **6. References**

538 Allen, S.E., Durrieu de Madron, X., 2009. A review of the role of submarine canyons in
539 deep-ocean exchange with the shelf. Ocean Sci. 5, 607–620.
540 https://doi.org/10.5194/os-5-607-2009.

541 Azpiroz-Zabala, M., Cartigny, M.J.B., Talling, P.J., Parsons, D.R., Sumner, E.J., Clare,
542 M.A., Simmons, S.M., Cooper, C., Pope, E.L., 2017. Newly recognized turbidity
543 current structure can explain prolonged flushing of submarine canyons. Sci. Adv. 3,
544 e1700200. https://doi.org/10.1126/sciadv.1700200.
545 Babonneau, N., Savoye, B., Cremer, M., Klein, B., 2002. Morphology and architecture of
546 the present canyon and channel system of the Zaire deep-sea fan. Mar. Pet. Geol.
547 19, 445–467. https://doi.org/10.1016/S0264-8172(02)00009-0.
548 Bassetti, M.A., Jouet, G., Dufois, F., Berné, S., Rabineau, M., Taviani, M., 2006. Sand
549 bodies at the shelf edge in the Gulf of Lions (Western Mediterranean): Deglacial
550 history and modern processes. Mar. Geol., EUROSTRATAFORM VOL. 1: Source
551 to Sink Sedimentation on the European Margin 234, 93–109.
552 https://doi.org/10.1016/j.margeo.2006.09.010.
553 Bayon, G., De Deckker, P., Magee, J.W., Germain, Y., Bermell, S., Tachikawa, K.,
554 Norman, M.D., 2017. Extensive wet episodes in Late Glacial Australia resulting
555 from high-latitude forcings. Sci. Rep. 7, 1–7. https://doi.org/10.1038/srep44054.
556 Bayon G., Douglas G.B., Denton G.J., Monin L., De Deckker P. 2020. Preferential
557 Riverine Export of Fine Volcanogenic Particles to the Southeast Australian Margin.
558 Frontiers in Marine Science 7, 89. https://doi: 10.3389/fmars.2020.00089.
559 Belyaeva, N.V., Burmistrova, I.I., 1985. Critical carbonate levels in the Indian Ocean. J.
560 Foraminifer. Res. 15, 337–341. https://doi.org/10.2113/gsjfr.15.4.337.
561 Bernhardt, A., Hebbeln, D., Regenberg, M., Lückge, A., Strecker, M.R., 2016. Shelfal
562 sediment transport by an undercurrent forces turbidity current activity during high

563 sea level along the Chile continental margin. Geology 44, 295–298.
564 https://doi.org/10.1130/G37594.1.
565 Bouma, A.H., Kuenen, P.H., Shepard, F.P., 1962. Sedimentology of some Flysch
566 deposits: a graphic approach to facies interpretation. Amsterdam: Elsevier.
567 Bouma, A.H., Normark, W.R., Barnes, N.E. (Eds.), 1985. Submarine Fans and Related
568 Turbidite Systems, Frontiers in Sedimentary Geology. Springer-Verlag, New York.
569 Bourillet, Jj.-F., Reynaud, J.-Y., Baltzer, A., Zaragosi, S., 2003. The 'Fleuve Manche':
570 the submarine sedimentary features from the outer shelf to the deep-sea fans. J.
571 Quat. Sci. 18, 261–282. https://doi.org/10.1002/jqs.757.
572 Bourman, R.P., Murray-Wallace, C.V., Harvey, N., 2016. Explaining the coastal
573 landscapes of South Australia — A synthesis, in: Coastal Landscapes of South
574 Australia. University of Adelaide Press, pp. 387–405.
575 Calvo, E., Pelejero, C., De Deckker, P., Logan, G.A., 2007. Antarctic deglacial pattern in
576 a 30 kyr record of sea surface temperature offshore South Australia. Geophys. Res.
577 Lett. 34, L13707. https://doi.org/10.1029/2007GL029937.
578 Covault, J.A., Graham, S.A., 2010. Submarine fans at all sea-level stands: Tectono-
579 morphologic and climatic controls on terrigenous sediment delivery to the deep sea.
580 Geology 38, 939–942. https://doi.org/10.1130/G31081.1.
581 Cresswell, G.R., Peterson, J.L., 1993. The Leeuwin Current south of Western Australia.
582 Mar. Freshw. Res. 44, 285–303. https://doi.org/10.1071/mf9930285.
583 De Deckker, P., Moros, M., Perner, K., Jansen, E., 2012. Influence of the tropics and
584 southern westerlies on glacial interhemispheric asymmetry. Nat. Geosci. 5, 266–
585 269. https://doi.org/10.1038/ngeo1431.

de Garidel-Thoron, T., Beaufort, L., Bassinot, F., Henry, P., 2004. Evidence for large methane releases to the atmosphere from deep-sea gas-hydrate dissociation during the last glacial episode. Proc. Natl. Acad. Sci. 101, 9187–9192. https://doi.org/10.1073/pnas.0402909101.

Debenay, J.P., 2012. A guide to 1,000 foraminifera from southwestern Pacific: New Caledonia. Marseille IRD Éditions, Institut de recherche pour le développement Paris Muséum national d'histoire naturelle.

Durand, M., Mojtahid, M., Maillet, G.M., Baltzer, A., Schmidt, S., Blet, S., Marchès, E., Howa, H., 2018. Late Holocene record from a Loire River incised paleovalley (French inner continental shelf): Insights into regional and global forcing factors. Palaeogeogr. Palaeoclimatol. Palaeoecol. 511, 12–28. https://doi.org/10.1016/j.palaeo.2018.06.035.

Duros, P., Fontanier, C., de Stigter, H.C., Cesbron, F., Metzger, E., Jorissen, F.J., 2012. Live and dead benthic foraminiferal faunas from Whittard Canyon (NE Atlantic): Focus on taphonomic processes and paleo-environmental applications. Mar. Micropaleontol. 94–95, 25–44. https://doi.org/10.1016/j.marmicro.2012.05.004.

Dutkiewicz, A., Müller, R.D., O'Callaghan, S., Jónasson, H., 2015. Census of seafloor sediments in the world's ocean. Geology 43, 795–798. https://doi.org/10.1130/G36883.1.

Emery, W.J., Meincke, J., 1986. Global water masses: summary and review. Glob. Water Masses Summ. Rev. 9, 383–391.

607 Feary, D.A., Birch, G., Boreen, T., Chudyk, E., Lanyon, R., Petkovic, P., Shafik, S., 1993.
608 Geological Sampling in the Great Australian Bight: Scientific Post-cruise Report -
609 R/V Rig Seismic Cruise 102 - (No. 18), Geoscience Australia Record.
610 Felix, M., Sturton, S., Peakall, J., 2005. Combined measurements of velocity and
611 concentration in experimental turbidity currents. Sediment. Geol., 179, 31–47.
612 https://doi.org/10.1016/j.sedgeo.2005.04.008.
613 Fernandez-Arcaya, U., Ramirez-Llodra, E., Aguzzi, J., Allcock, A.L., Davies, J.S.,
614 Dissanayake, A., Harris, P., Howell, K., Huvenne, V.A.I., Macmillan-Lawler, M.,
615 Martín, J., Menot, L., Nizinski, M., Puig, P., Rowden, A.A., Sanchez, F., Van den
616 Beld, I.M.J., 2017. Ecological Role of Submarine Canyons and Need for Canyon
617 Conservation: A Review. Front. Mar. Sci. 4.
618 https://doi.org/10.3389/fmars.2017.00005.
619 Galy, V., France-Lanord, C., Beyssac, O., Faure, P., Kudrass, H., Palhol, F., 2007.
620 Efficient organic carbon burial in the Bengal fan sustained by the Himalayan
621 erosional system.
622 Garcia, J., Mojtahid, M., Howa, H., Michel, E., Schiebel, R., Charbonnier, C., Jorissen,
623 F.J., 2013. Benthic and Planktic Foraminifera as Indicators of Late Glacial to
624 Holocene Paleoclimatic Changes in a Marginal Environment: An Example from the
625 Southeastern Bay of Biscay. Acta Protozool. 52, 161–180.
626 Gingele, F., De Deckker, P., Norman, M., 2007. Late Pleistocene and Holocene climate
627 of SE Australia reconstructed from dust and river loads deposited offshore the
628 River Murray Mouth. Earth Planet. Sci. Lett. 255, 257–272.
629 https://doi.org/10.1016/j.epsl.2006.12.019.

630 Gingele, F.X., De Deckker, P., 2005. Late Quaternary fluctuations of palaeoproductivity
631 in the Murray Canyons area, South Australian continental margin. Palaeogeogr.
632 Palaeoclimatol. Palaeoecol. 220, 361–373.
633 https://doi.org/10.1016/j.palaeo.2005.01.012.
634 Gingele, F.X., De Deckker, P., Hillenbrand, C.-D., 2004. Late Quaternary terrigenous
635 sediments from the Murray Canyons area, offshore South Australia and their
636 implications for sea level change, palaeoclimate and palaeodrainage of the Murray–
637 Darling Basin. Mar. Geol. 212, 183–197.
638 https://doi.org/10.1016/j.margeo.2004.09.001
639 Grafton, R.Q., Pittock, J., Williams, J., Jiang, Q., Possingham, H., Quiggin, J., 2014.
640 Water Planning and Hydro-Climatic Change in the Murray-Darling Basin,
641 Australia. AMBIO 43, 1082–1092. https://doi.org/10.1007/s13280-014-0495-x.
642 Hayward, B.W., Grenfell, H.R., Ashwaq, T.S., Helen, L.N., Martin, A.B., 2010. Recent
643 New Zealand deep-water benthic foraminifera: taxonomy, ecologic distribution,
644 biogeography, and use in paleoenvironmental assessment, GNS Science monograph.
645 New Zealand Geological Survey Paleontological Bulletin.
646 Hayward, B.W., Sabaa, A., Grenfell, H.R., 2004. Benthic foraminifera and the late
647 Quaternary (last 150 ka) paleoceanographic and sedimentary history of the Bounty
648 Trough, east of New Zealand. Palaeogeogr. Palaeoclimatol. Palaeoecol. 211, 59–93.
649 https://doi.org/10.1016/j.palaeo.2004.04.007.
650 Hayward, B.W., Sabaa, A.T., Triggs, C.M., 2019. Using foraminiferal test-size
651 distribution and other methods to recognise Quaternary bathyal turbidites and

652 taphonomically-modified faunas. Mar. Micropaleontol. 148, 65–77.
653 https://doi.org/10.1016/j.marmicro.2019.03.008.
654 Hayward, W.B., Grenfell, H.R., Reid, C.M., Hayward, K.A., 1999. Recent New Zealand
655 shallow-water benthic foraminifera: Taxonomy, ecologic distribution,
656 biogeography, and use in paleoenvironmental assessment. Institute of Geological &
657 Nuclear Sciences monograph.
658 Henrich, R., Cherubini, Y., Meggers, H., 2010. Climate and sea level induced turbidite
659 activity in a canyon system offshore the hyperarid Western Sahara (Mauritania):
660 The Timiris Canyon. Mar. Geol. 275, 178–198.
661 https://doi.org/10.1016/j.margeo.2010.05.011.
662 Hill, P.J., De Deckker, P., 2004. AUSCAN seafloor mapping and geological sampling
663 survey on the Australian southern margin by RV Marion Dufresne in 2003: Final
664 project report, Geoscience Australia Record. (Petroleum and Marine Division).
665 Hill, P.J., Deckker, P. de, Exon, N.F., 2005. Geomorphology and evolution of the
666 gigantic Murray canyons on the Australian southern margin. Aust. J. Earth Sci. 52,
667 117–136. https://doi.org/10.1080/08120090500100085.
668 Hill, P.J., Deckker†, P.D., Borch, C. von der, Murray-Wallace, C.V., 2009. Ancestral
669 Murray River on the Lacepede Shelf, southern Australia: Late Quaternary
670 migrations of a major river outlet and strandline development. Aust. J. Earth Sci. 56,
671 135–157. https://doi.org/10.1080/08120090802546993.
672 Hogg, A.G., Hua, Q., Blackwell, P.G., Niu, M., Buck, C.E., Guilderson, T.P., Heaton,
673 T.J., Palmer, J.G., Reimer, P.J., Reimer, R.W., Turney, C.S.M., Zimmerman,

674 S.R.H., 2013. SHCal13 Southern Hemisphere Calibration, 0–50,000 Years cal BP.
675 Radiocarbon 55, 1889–1903. https://doi.org/10.2458/azu_js_rc.55.16783.
676 James, N.P., Bone, Y., Kyser, T.K., 2005. Where Has All the Aragonite Gone?
677 Mineralogy of Holocene Neritic Cool-Water Carbonates, Southern Australia. J.
678 Sediment. Res. 75, 454–463. https://doi.org/10.2110/jsr.2005.035.
679 James, N.P., Boreen, T.D., Bone, Y., Feary, D.A., 1994. Holocene carbonate
680 sedimentation on the west Eucla Shelf, Great Australian Bight: a shaved shelf.
681 Sediment. Geol. 90, 161–177. https://doi.org/10.1016/0037-0738(94)90037-X.
682 James, N.P., Bone, Y., 2011. Neritic Carbonate Sediments in a Temperate Realm:
683 Southern Australia. Springer, Dordrecht, The Netherlands., pp. 254.
684 https://doi.org/10.1007/978-90-481-9289-2.James, N.P., Reid, C.M., Bone, Y.,
685 Levings, A., Malcolm, I., 2013. The macroalgal carbonate factory at a cool-to-
686 warm temperate marine transition, Southern Australia. Sediment. Geol. 291, 1–26.
687 https://doi.org/10.1016/j.sedgeo.2013.03.007.
688 Jorissen, F., Wittling, I., 1999. Ecological evidence from live–dead comparisons of
689 benthic foraminiferal faunas off Cape Blanc (Northwest Africa). Palaeogeogr.
690 Palaeoclimatol. Palaeoecol. 149, 151–170. https://doi.org/10.1016/S0031-
691 0182(98)00198-9
692 Kanner, L.C., Burns, S.J., Cheng, H., Edwards, R.L., 2012. High-Latitude Forcing of the
693 South American Summer Monsoon During the Last Glacial. Science 335, 570–573.
694 https://doi.org/10.1126/science.1213397.

695 Lambeck, K., Rouby, H., Purcell, A., Sun, Y., Sambridge, M., 2014. Sea level and global
696 ice volumes from the Last Glacial Maximum to the Holocene. Proc. Natl. Acad. Sci.
697 111, 15296–15303. https://doi.org/10.1073/pnas.1411762111.
698 Lastras, G., Arzola, R.G., Masson, D.G., Wynn, R.B., Huvenne, V.A.I., Hühnerbach, V.,
699 Canals, M., 2009. Geomorphology and sedimentary features in the Central
700 Portuguese submarine canyons, Western Iberian margin. Geomorphology 103,
701 310–329. https://doi.org/10.1016/j.geomorph.2008.06.013.
702 Lebreiro, S.M., Voelker, A.H.L., Vizcaino, A., Abrantes, F.G., Alt-Epping, U., Jung, S.,
703 Thouveny, N., Gràcia, E., 2009. Sediment instability on the Portuguese continental
704 margin under abrupt glacial climate changes (last 60kyr). Quat. Sci. Rev. 28, 3211–
705 3223. https://doi.org/10.1016/j.quascirev.2009.08.007.
706 Li, F., Griffiths, C.M., Dyt, C.P., Weill, P., Feng, M., Salles, T., Jenkins, C., 2009.
707 Multigrain seabed sediment transport modelling for the south-west Australian Shelf.
708 Mar. Freshw. Res. 60, 774–785. https://doi.org/10.1071/MF08049.
709 Li, Q., McGowran, B., James, N.P., Bone, Y., Cann, J.H., 1996. Mixed Foraminiferal
710 Biofacies on the Mesotrophic, Mid-Latitude Lacepede Shelf, South Australia.
711 PALAIOS 11, 176. https://doi.org/10.2307/3515069
712 Lombo Tombo, S., Dennielou, B., Berné, S., Bassetti, M.-A., Toucanne, S., Jorry, S.J.,
713 Jouet, G., Fontanier, C., 2015. Sea-level control on turbidite activity in the Rhone
714 canyon and the upper fan during the Last Glacial Maximum and Early deglacial.
715 Sediment. Geol. 323, 148–166. https://doi.org/10.1016/j.sedgeo.2015.04.009.
716 Lopes dos Santos, R.A., Spooner, M.I., Barrows, T.T., De Deckker, P., Damsté, J.S.S.,
717 Schouten, S., 2013. Comparison of organic (UK'37, TEXH86, LDI) and faunal

718 proxies (foraminiferal assemblages) for reconstruction of late Quaternary sea
719 surface temperature variability from offshore southeastern Australia.
720 Paleoceanography 28, 377–387. https://doi.org/10.1002/palo.20035.
721 Lopes dos Santos, R.A., Wilkins, D., De Deckker, P., Schouten, S., 2012. Late
722 Quaternary productivity changes from offshore Southeastern Australia: A
723 biomarker approach. Palaeogeogr. Palaeoclimatol. Palaeoecol. 363–364, 48–56.
724 https://doi.org/10.1016/j.palaeo.2012.08.013.
725 Lowe, D.R., 1982. Sediment gravity flows; II, Depositional models with special reference
726 to the deposits of high-density turbidity currents. J. Sediment. Res. 52, 279–297.
727 https://doi.org/10.1306/212F7F31-2B24-11D7-8648000102C1865D.
728 Mallet, C.D., Heezen, B.C., 1977. Circum-Polar Circulation and Late Tertiary Changes in
729 the Carbonate Compensation Depth South of Australia**Contribution No. 2373 of
730 the Lamont-Doherty Geological Observatory., in: Heezen, B.C. (Ed.),
731 Developments in Sedimentology, Influence of Abyssal Circulation on Sedimentary
732 Accumulations in Space and Time. Elsevier, pp. 89–101.
733 https://doi.org/10.1016/S0070-4571(08)70552-1.
734 Mauffrey, M.A., Berné, S., Jouet, G., Giresse, P., Gaudin, M., 2015. Sea-level control on
735 the connection between shelf-edge deltas and the Bourcart canyon head (western
736 Mediterranean) during the last glacial/interglacial cycle. Mar. Geol. 370, 1–19.
737 https://doi.org/10.1016/j.margeo.2015.09.010.
738 McClain, C.R., Barry, J.P., 2010. Habitat heterogeneity, disturbance, and productivity
739 work in concert to regulate biodiversity in deep submarine canyons. Ecology 91,
740 964–976. https://doi.org/10.1890/09-0087.1.

741 Middleton, G.V., Hampton, M.A., 1973. Sediment gravity flows: mechanics of flow and
742 deposition, in: Turbidites and Deep-Water Sedimentation, SEPM Pacific Section
743 Short Course. Anaheim, California, pp. 1–38.
744 Middleton, J.F., Bye, J.A.T., 2007. A review of the shelf-slope circulation along
745 Australia's southern shelves: Cape Leeuwin to Portland. Prog. Oceanogr. 75, 1–41.
746 https://doi.org/10.1016/j.pocean.2007.07.001.
747 Mojtahid, M., Geslin, E., Coynel, A., Gorse, L., Vella, C., Davranche, A., Zozzolo, L.,
748 Blanchet, L., Bénéteau, E., Maillet, G., 2016. Spatial distribution of living (Rose
749 Bengal stained) benthic foraminifera in the Loire estuary (western France). J. Sea
750 Res., Recent and past sedimentary, biogeochemical and benthic ecosystem
751 evolution of the Loire Estuary (Western France) 118, 1–16.
752 https://doi.org/10.1016/j.seares.2016.02.003
753 Mojtahid, M., Griveaud, C., Fontanier, C., Anschutz, P., Jorissen, F.J., 2010. Live benthic
754 foraminiferal faunas along a bathymetrical transect (140–4800 m) in the Bay of
755 Biscay (NE Atlantic). Rev. Micropaléontologie 53, 139–162.
756 https://doi.org/10.1016/j.revmic.2010.01.002
757 Mojtahid, M., Jorissen, F.J., Garcia, J., Schiebel, R., Michel, E., Eynaud, F., Gillet, H.,
758 Cremer, M., Diz Ferreiro, P., Siccha, M., Howa, H., 2013. High resolution
759 Holocene record in the southeastern Bay of Biscay: Global versus regional climate
760 signals. Palaeogeogr. Palaeoclimatol. Palaeoecol. 377, 28–44.
761 https://doi.org/10.1016/j.palaeo.2013.03.004
762 Moros, M., De Deckker, P., Jansen, E., Perner, K., Telford, R.J., 2009. Holocene climate
763 variability in the Southern Ocean recorded in a deep-sea sediment core off South

764 Australia. Quat. Sci. Rev. 28, 1932–1940.
765 https://doi.org/10.1016/j.quascirev.2009.04.007.
766 Mountjoy, J.J., Barnes, P.M., Pettinga, J.R., 2009. Morphostructure and evolution of
767 submarine canyons across an active margin: Cook Strait sector of the Hikurangi
768 Margin, New Zealand. Mar. Geol. 260, 45–68.
769 https://doi.org/10.1016/j.margeo.2009.01.006.
770 Mueller, D., Jacobs, Z., Cohen, T.J., Price, D.M., Reinfelds, I.V., Shulmeister, J., 2018.
771 Revisiting an arid LGM using fluvial archives: a luminescence chronology for
772 palaeochannels of the Murrumbidgee River, south-eastern Australia. J. Quat. Sci.
773 33, 777–793. https://doi.org/10.1002/jqs.3059.
774 Mulder, T., Cirac, P., Gaudin, M., Bourillet, J.-F., Trainer, J., Normand, A., Weber, O.,
775 Griboulard, R., Jouanneau, J.-M., Anschutz, P., Jorissen, F.J., 2004. Understanding
776 continent-ocean sediment transfer. Eos Trans. Am. Geophys. Union 85, 257–262.
777 https://doi.org/10.1029/2004EO270001.
778 Mulder, T., Savoye, B., Syvitski, J., Parize, O., 1997. Des courants de turbidité
779 hyperpycnaux dans la tête du canyon du Var ? Données hydrologiques et
780 observations de terrain. Oceanol. Acta 20, 607–626.
781 Mulder, T., Syvitski, J.P.M., 1995. Turbidity Currents Generated at River Mouths during
782 Exceptional Discharges to the World Oceans. J. Geol. 103, 285–299.
783 Mulder, T., Syvitski, J.P.M., Migeon, S., Faugères, J.-C., Savoye, B., 2003. Marine
784 hyperpycnal flows: initiation, behavior and related deposits. A review. Mar. Pet.
785 Geol., Turbidites: Models and Problems 20, 861–882.
786 https://doi.org/10.1016/j.marpetgeo.2003.01.003.

787 Mulder, T., Zaragosi, S., Garlan, T., Mavel, J., Cremer, M., Sottolichio, A., Sénéchal, N.,
788 Schmidt, S., 2012. Present deep-submarine canyons activity in the Bay of Biscay
789 (NE Atlantic). Mar. Geol. 295–298, 113–127.
790 https://doi.org/10.1016/j.margeo.2011.12.005.
791 Munsell, A.H., 1912. A Pigment Color System and Notation. Am. J. Psychol. 23, 236–
792 244. https://doi.org/10.2307/1412843.
793 Murray, J., 2006. Ecology and Applications of Benthic Foraminifera. Cambridge:
794 Cambridge University Press. doi:10.1017/CBO9780511535529.
795 Nash, G.J., De Deckker, P., Mitchell, C., Murray-Wallace, C.V., Hua, Q., 2018.
796 Micropalaeontological evidence for deglacial marine flooding of the ancient
797 courses of the River Murray across the Lacepede Shelf, southern Australia. Mar.
798 Micropaleontol. 141, 55–72. https://doi.org/10.1016/j.marmicro.2018.04.002.
799 Parsons, J.D., Bush, J.W.M., Syvitski, J.P.M., 2001. Hyperpycnal plume formation from
800 riverine outflows with small sediment concentrations. Sedimentology 48, 465–478.
801 https://doi.org/10.1046/j.1365-3091.2001.00384.x.
802 Passlow, V., Pinxian, W., Chivas, A.R., 1997. Late Quaternary palaeoceanography near
803 Tasmania, southern Australia. Palaeogeogr. Palaeoclimatol. Palaeoecol., The Late
804 Quaternary Palaeoceanography of the Australasian Region 131, 433–463.
805 https://doi.org/10.1016/S0031-0182(97)00015-1.
806 Paull, C.K., Iii, W.U., Caress, D.W., Lundsten, E., Covault, J.A., Maier, K.L., Xu, J.,
807 Augenstein, S., 2010. Origins of large crescent-shaped bedforms within the axial
808 channel of Monterey Canyon, offshore California. Geosphere 6, 755–774.
809 https://doi.org/10.1130/GES00527.1.

Paull, C.K., McGann, M., Sumner, E.J., Barnes, P.M., Lundsten, E.M., Anderson, K., Gwiazda, R., Edwards, B., Caress, D.W., 2014. Sub-decadal turbidite frequency during the early Holocene: Eel Fan, offshore northern California. Geology 42, 855–858. https://doi.org/10.1130/G35768.1

Perner, K., Moros, M., De Deckker, P., Blanz, T., Wacker, L., Telford, R., Siegel, H., Schneider, R., Jansen, E., 2018. Heat export from the tropics drives mid to late Holocene palaeoceanographic changes offshore southern Australia. Quat. Sci. Rev. 180, 96–110. https://doi.org/10.1016/j.quascirev.2017.11.033.

Petherick, L., Bostock, H., Cohen, T.J., Fitzsimmons, K., Tibby, J., Fletcher, M.-S., Moss, P., Reeves, J., Mooney, S., Barrows, T., Kemp, J., Jansen, J., Nanson, G., Dosseto, A., 2013. Climatic records over the past 30 ka from temperate Australia – a synthesis from the Oz-INTIMATE workgroup. Quat. Sci. Rev., Linking Southern Hemisphere records and past circulation patterns: the AUS-INTIMATE project 74, 58–77. https://doi.org/10.1016/j.quascirev.2012.12.012.

Pierau, R., Hanebuth, T.J.J., Krastel, S., Henrich, R., 2010. Late Quaternary climatic events and sea-level changes recorded by turbidite activity, Dakar Canyon, NW Africa. Quat. Res. 73, 385–392. https://doi.org/10.1016/j.yqres.2009.07.010.

Piper, D.J.W., Normark, W.R., 2009. Processes That Initiate Turbidity Currents and Their Influence on Turbidites: A Marine Geology Perspective. J. Sediment. Res. 79, 347–362. https://doi.org/10.2110/jsr.2009.046.

Quattrini, A.M., Nizinski, M.S., Chaytor, J.D., Demopoulos, A.W.J., Roark, E.B., France, S.C., Moore, J.A., Heyl, T., Auster, P.J., Kinlan, B., Ruppel, C., Elliott, K.P., Kennedy, B.R.C., Lobecker, E., Skarke, A., Shank, T.M., 2015. Exploration of the

Canyon-Incised Continental Margin of the Northeastern United States Reveals Dynamic Habitats and Diverse Communities. PLOS ONE 10, e0139904. https://doi.org/10.1371/journal.pone.0139904.

Reeves, J.M., Barrows, T.T., Cohen, T.J., Kiem, A.S., Bostock, H.C., Fitzsimmons, K.E., Jansen, J.D., Kemp, J., Krause, C., Petherick, L., Phipps, S.J., 2013. Climate variability over the last 35,000 years recorded in marine and terrestrial archives in the Australian region: an OZ-INTIMATE compilation. Quat. Sci. Rev., 74, 21–34. https://doi.org/10.1016/j.quascirev.2013.01.001.

Reimer, P.J., Bard, E., Bayliss, A., Beck, J.W., Blackwell, P.G., Ramsey, C.B., Buck, C.E., Cheng, H., Edwards, R.L., Friedrich, M., Grootes, P.M., Guilderson, T.P., Haflidason, H., Hajdas, I., Hatté, C., Heaton, T.J., Hoffmann, D.L., Hogg, A.G., Hughen, K.A., Kaiser, K.F., Kromer, B., Manning, S.W., Niu, M., Reimer, R.W., Richards, D.A., Scott, E.M., Southon, J.R., Staff, R.A., Turney, C.S.M., Plicht, J. van der, 2013. IntCal13 and Marine13 Radiocarbon Age Calibration Curves 0–50,000 Years cal BP. Radiocarbon 55, 1869–1887. https://doi.org/10.2458/azu_js_rc.55.16947.

Richardson, L.E., Middleton, J.F., Kyser, T.K., James, N.P., Opdyke, B.N., 2019. Shallow water masses and their connectivity along the southern Australian continental margin. Deep Sea Res. Oceanogr. 152, 103083. https://doi.org/10.1016/j.dsr.2019.103083.

Schlünz, B., Schneider, R.R., 2000. Transport of terrestrial organic carbon to the oceans by rivers: re-estimating flux- and burial rates. Int. J. Earth Sci. 88, 599–606. https://doi.org/10.1007/s005310050290.

856 Schmidt, S., De Deckker, P., Etcheber, H., Caradec, S., 2010. Are the Murray Canyons
857 offshore southern Australia still active for sediment transport? Geol. Soc. Lond.
858 Spec. Publ. 346, 43–55. https://doi.org/10.1144/SP346.4.
859 Schröder-Adams, C.J., Boyd, R., Ruming, K., Sandstrom, M., 2008. Influence of
860 sediment transport dynamics and ocean floor morphology on benthic foraminifera,
861 offshore Fraser Island, Australia. Mar. Geol. 254, 47–61.
862 https://doi.org/10.1016/j.margeo.2008.05.002.
863 Shanmugam, G., 2018. The hyperpycnite problem. J. Palaeogeogr. 7, 6.
864 https://doi.org/10.1186/s42501-018-0001-7.
865 Shanmugam, G., 1997. The Bouma Sequence and the turbidite mind set. Earth-Sci. Rev.
866 42, 201–229. https://doi.org/10.1016/S0012-8252(97)81858-2.
867 Shepard, F.P., 1972. Submarine canyons. Earth-Sci. Rev. 8, 1–12.
868 https://doi.org/10.1016/0012-8252(72)90032-3.
869 Sprigg, C., 1948. Newly Discovered Submarine Canyons of New Guinea and South
870 Australia. Nature 161, 246–247. https://doi.org/10.1038/161246b0.
871 Strachan, L.J., Bostock, H.C., Barnes, P.M., Neil, H.L., Gosling, M., 2016. Non-cohesive
872 silt turbidity current flow processes; insights from proximal sandy-silt and silty-
873 sand turbidites, Fiordland, New Zealand. Sediment. Geol. 342, 118–132.
874 https://doi.org/10.1016/j.sedgeo.2016.06.017.
875 Tisnérat-Laborde, N., Poupeau, J.J., Tannau, J.F., Paterne, M., 2001. Development of a
876 semi-automated system for routine preparation of carbonate samples. Radiocarbon
877 43, 299–304.

878 Turney, C.S.M., Palmer, J., Bronk Ramsey, C., Adolphi, F., Muscheler, R., Hughen, K.A.,
879 Staff, R.A., Jones, R.T., Thomas, Z.A., Fogwill, C.J., Hogg, A., 2016. High-
880 precision dating and correlation of ice, marine and terrestrial sequences spanning
881 Heinrich Event 3: Testing mechanisms of interhemispheric change using New
882 Zealand ancient kauri (*Agathis australis*). Quat. Sci. Rev. 137, 126–134.
883 https://doi.org/10.1016/j.quascirev.2016.02.005.
884 Waelbroeck, C., Labeyrie, L., Michel, E., Duplessy, J.C., McManus, J.F., Lambeck, K.,
885 Balbon, E., Labracherie, M., 2002. Sea-level and deep water temperature changes
886 derived from benthic foraminifera isotopic records. Quat. Sci. Rev. 21, 295–305.
887 https://doi.org/10.1016/S0277-3791(01)00101-9.
888 Walker, R.G., 1976. Facies Models 2. Turbidites and Associated Coarse Clastic Deposits.
889 Geosci. Can. 3, 25–36.
890 Wang, L., 2000. Isotopic signals in two morphotypes of *Globigerinoides ruber* (white)
891 from the South China Sea: implications for monsoon climate change during the last
892 glacial cycle. Palaeogeogr. Palaeoclimatol. Palaeoecol. 161, 381–394.
893 https://doi.org/10.1016/S0031-0182(00)00094-8.
894 Weaver, P.P.E., Wynn, R.B., Kenyon, N.H., Evans, J., 2000. Continental margin
895 sedimentation, with special reference to the north-east Atlantic margin.
896 Sedimentology 47, 239–256. https://doi.org/10.1046/j.1365-
897 3091.2000.0470s1239.x.
898 Wendt, K.A., Häuselmann, A.D., Fleitmann, D., Berry, A.E., Wang, X., Auler, A.S.,
899 Cheng, H., Edwards, R.L., 2019. Three-phased Heinrich Stadial 4 recorded in NE

Brazil stalagmites. Earth Planet. Sci. Lett. 510, 94–102. https://doi.org/10.1016/j.epsl.2018.12.025.

Williams, M.A.J., Pal, J.N., Jaiswal, M., Singhvi, A.K., 2006. River response to Quaternary climatic fluctuations: evidence from the Son and Belan valleys, north-central India. Quat. Sci. Rev. 25, 2619–2631. https://doi.org/10.1016/j.quascirev.2005.07.018.

Woo, M., Pattiaratchi, C., 2008. Hydrography and water masses off the western Australian coast. Deep Sea Res. Part Oceanogr. Res. Pap. 55, 1090–1104. https://doi.org/10.1016/j.dsr.2008.05.005.

Wright, L.D., Friedrichs, C.T., 2006. Gravity-driven sediment transport on continental shelves: A status report. Cont. Shelf Res., Special Issue in Honor of Richard W. Sternberg's Contributions to Marine Sedimentology 26, 2092–2107. https://doi.org/10.1016/j.csr.2006.07.008.

Zaragosi, S., Bourillet, J.-F., Eynaud, F., Toucanne, S., Denhard, B., Toer, A.V., Lanfumey, V., 2006. The impact of the last European deglaciation on the deep-sea turbidite systems of the Celtic-Armorican margin (Bay of Biscay). Geo-Mar. Lett. 26, 317–329. https://doi.org/10.1007/s00367-006-0048-9.

Zaragosi, S., Eynaud, F., Pujol, C., Auffret, G.A., Turon, J.-L., Garlan, T., 2001. Initiation of the European deglaciation as recorded in the northwestern Bay of Biscay slope environments (Meriadzek Terrace and Trevelyan Escarpment): a multi-proxy approach. Earth Planet. Sci. Lett. 188, 493–507. https://doi.org/10.1016/S0012-821X(01)00332-6.

922 Zavala, C., Arcuri, M., Di Megli, M., Gamero Dia, H., Contreras, C., 2011. A Genetic
923 Facies Tract for theAnalysis of Sustained HyperpycnalFlow Deposits, in: Sediment
924 Transfer Fromshelf to Deep Water —Revisiting the Delivery System, AAPG
925 Studies in Geology. pp. 31 – 51.

926

927 **Table caption**

928

929 **Table 1.** Radiocarbon dates, calibrated ages (cal. year BP; 2 sigma) and their
930 corresponding sediment depths and dated material listing species used.

931

932 **Figures caption**

933

934 **Figure 1.** a) Map showing the location of the study area at the outlet of one of Australia's
935 largest river systems, the Murray–Darling Basin after Hill et al. (2009) as well as the
936 main currents and water masses south of Australia according to Richardson et al. (2019)
937 and https://www.csiro.au/. Water masses: TSW – Tropical Surface Water, SICW – South
938 Indian Central Water, STSW – Subtropical Surface Water. Map adapted from
939 https://maps.ngdc.noaa.gov/viewers/bathymetry/. b) 3-D morphobathymetric map of the
940 Murray Canyon Group generated from swath mapping data gathered during several
941 cruises (Hill and De Deckker, 2004) and updated with additional information gathered
942 during the RV *Southern Surveyor* cruise SS02/06 showing their incised topography. Note
943 the presence of deep holes in the abyssal plain where the study core SS02/06-GC2 is
944 located. The red color indicates water depths < 200 m, yellow >200 m and <1000 m,

945 green >1000 m and <4000 m, and blue >4000 m; c) Water mass salinity profiles (grouped
946 in the hatched area), showing boundaries of Subantarctic Mode Water (SAMW),
947 Antarctic Intermediate Water (AAIW), upper and lower Circumpolar Deep Water
948 (CPDW) and Antarctic Bottom Water (AABW). Data are taken from the region adjacent
949 to the southeastern Australian mainland (36°S-42°S, 134°E-144°E) and south of
950 Tasmania (44°S-50°S, 144°E-149°E) after Passlow et al. (1997).
951
952 **Figure 2.** From left to right: Photography and interpretative lithological logs of core
953 SS02/06-GC02 and a descriptive curve of the three main grain size fractions (clay, silt
954 and sand) based on sedimentological visual observation. Position in the core of the
955 calibrated ^{14}C dates are shown in red. The sediment colours (e.g. 10YR/6/2) were
956 determined using a Munsell color chart (Munsell, 1912). The white dots indicate sample
957 locations. The yellow dots indicate the samples with some sediment loss that could not be
958 quantified for their foraminiferal content.
959
960 **Figure 3.** a) PCA analyses based on the percentages of the main benthic foraminiferal
961 species (i.e. present with ≥5% in at least one of the sediment samples); b) The modern
962 bathymetric distribution of the main benthic foraminiferal species, mostly after Hayward
963 et al. (1999, 2010).
964
965 **Figure 4.** Representation of the downcore Shannon index of biodiversity, the total
966 absolute densities of benthic foraminifera standardized to per gram of dry sediment and
967 species composition (only the main species occurring with ≥5% in at least one sample)

968 separated following the three PCA groups (see Figure 3). The interpretative lithological
969 logs and the descriptive curve of grain size are also represented.
970
971 **Figure 5.** Interpretative summary of the main results: a) The lithological logs. The yellow
972 dots indicate the samples with some sediment loss that could not be quantified for their
973 foraminiferal content; b) Interpretation of the grain-size curve in terms of Bouma
974 turbiditic sequences (Bs1 – Bs7). The climatic time periods referred to in the text are
975 indicated. HE: Heinrich Event; LGM: Last Glacial Maximum; c) The downcore Shannon
976 index and total absolute densities of benthic foraminifera standardized per gram of dry
977 sediment; d) Pie charts representing the cumulative percentages of the three main PCA
978 ecological groups, averaged for a number of sediment layers determined from Figure 4;
979 e) The typical Bouma sequence showing the T_a to T_e divisions (Bouma et al., 1962),
980 reinterpreted by other authors (Middleton and Hampton, 1973; Lowe, 1982; Shanmugan,
981 1997).
982
983 **Figure 6.** Interpretative summary scheme of the hydro-sedimentary processes leading the
984 deposition of the Bouma-like sequences in core SS2-CG2. Figure 6 is modified from
985 Mulder et al. (1997).
986
987 **Tables caption**
988
989 **Plate 1.** SEM photographs of: 1-2) *Textularia pseudogramen*; 3) *Textularia stricta;*4)
990 *Spirotextularia fistulosa*; 5) *Textularia goesi*; 6) *Gaudryina convexa*; 7) *Eggerella* sp.; 8)

991 *Pyrgo inornata*; 9) *Pyrgo denticulata*; 10) *Pyrgo depressa*; 11) *Pyrgo oblonga*; 12-14)
992 *Nummulopyrgo globulus*; 15) *Pseudomassilina* sp.1; 16) *Quinqueloculina* sp.; 17)
993 *Miliolinella fichteliana?*; 18-19) *Quinqueloculina auberiana*; 20) *Quinqueloculina*
994 *cuvieriana*; 21-22) *Quinqueloculina seminula*.
995
996 **Plate 2.** SEM photographs of: 23) *Laevidentalina inornata?* ; 24) *Lagena spicata*; 25)
997 *Mychostomina lucida* ; 26-27) *Pileolina zealandica* ; 28) *Siphogenerina raphana*; 29)
998 *Bolivina alata*; 30) *Bolivinita quadrilatera*; 31) *Bolivinellina pescicula*; 32) *Fursenkoina*
999 *schreibersiana*?; 33) *Bulimina marginata* f. *aculeata*; 34) *Bulimina striata*; 35) *Uvigerina*
1000 *mediterranea*; 36) *Uvigerina peregrina* s.l.; 37) *Trifarina angulosa*; 38) *Trifarina reussi*;
1001 39-40) *Pullenia quinqueloba*; 41) *Anomalinulla glabrata*; 42) *Nonion*
1002 *pacificum/Haynesina depressula ?*
1003
1004 **Plate 3.** SEM photographs of: 43-47) *Cibicidoides dispars* s.l. ; 48-52) *Cibicidoides*
1005 *wuellerstorfi*; 53-55) *Cibicides corticatus* ; 56) *Cibicides refulgens* ; 57) *Cibicides* sp. 1 ;
1006 58) *Cibicides* sp. 2 ; 59-63) *Cibicides variabilis ;* 64-66) *Cibicidoides pachyderma ;* 67-
1007 68) *Cibicides lobatulus*.
1008
1009 **Plate 4.** SEM photographs of: 69-71) *Gyroidina orbicularis;* 72-73) *Hoeglundina*
1010 *elegans;* 74) *Planulinoides biconcavus;* 75) *Rosalina globularis;* 76-78) *Astrononion*
1011 *novozealandicum;* 79) *Elphidium charlottense*?; 80) *Elphidium* sp.; 81-83) *Elphidium*
1012 *crispum;* 84-88) *Notorotalia clathrata*; 89-91) *Nuttallides bradyi*?*;* 92) *Evolvocassidulina*
1013 *belfordi;* 93-94) *Hemirobulina angistoma;* 95-96) *Sigmoidella elegantissima*

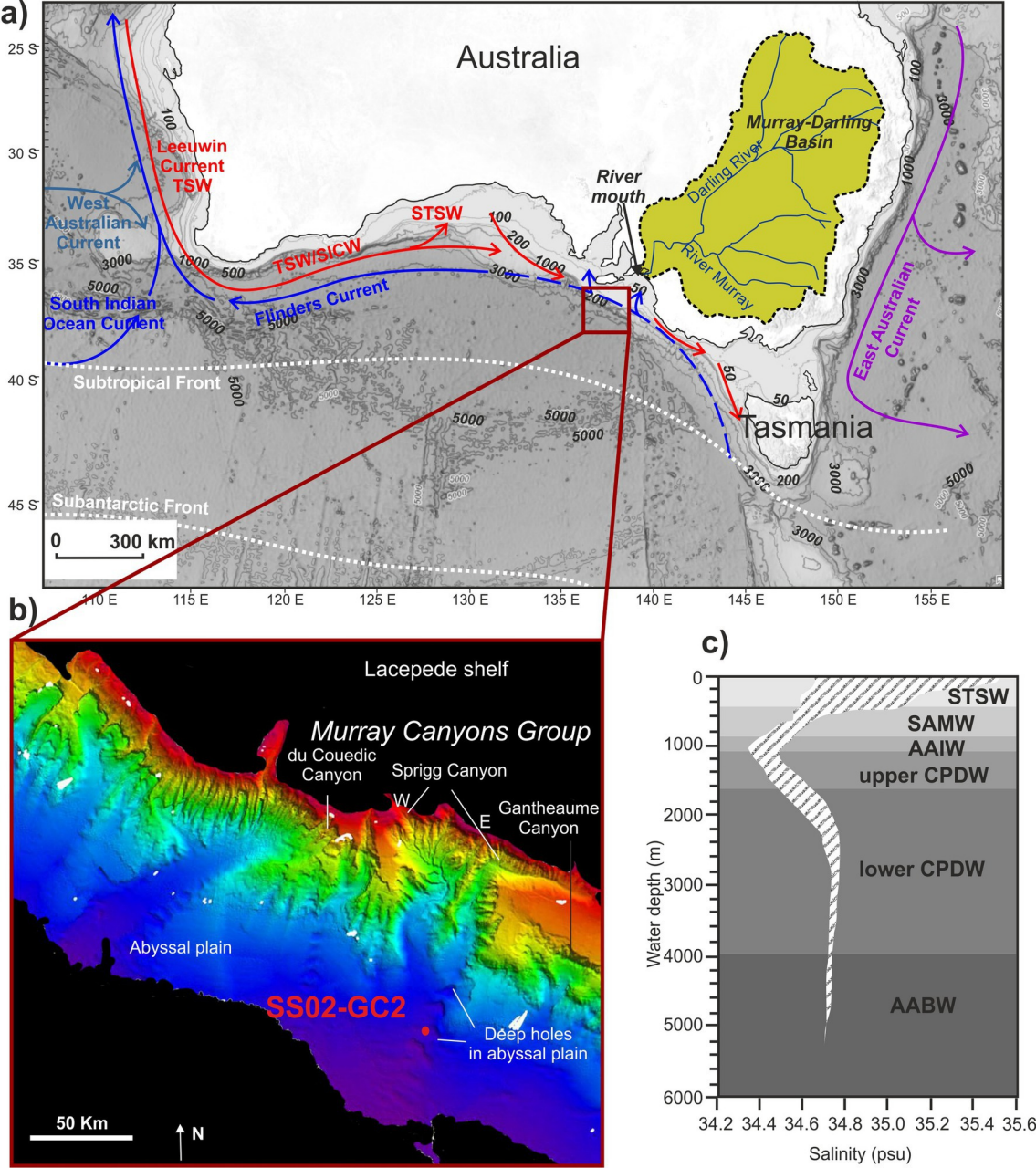
a)
Australia
Leeuwin Current TSW
West Australian Current
South Indian Ocean Current
STSW
TSW/SICW
Flinders Current
River mouth
Murray-Darling Basin
Darling River
River Murray
East Australian Current
Tasmania
Subtropical Front
Subantarctic Front
0 300 km
25 S
30 S
35 S
40 S
45 S
110 E
115 E
120 E
125 E
130 E
135 E
140 E
145 E
150 E
155 E
b)
Lacepede shelf
Murray Canyons Group
du Couedic Canyon
Sprigg Canyon
W
E
Gantheaume Canyon
Abyssal plain
SS02-GC2
Deep holes in abyssal plain
50 Km
N
c)
STSW
SAMW
AAIW
upper CPDW
lower CPDW
AABW
Water depth (m)
0
1000
2000
3000
4000
5000
6000
34.2
34.4
34.6
34.8
35.0
35.2
35.4
35.6
Salinity (psu)

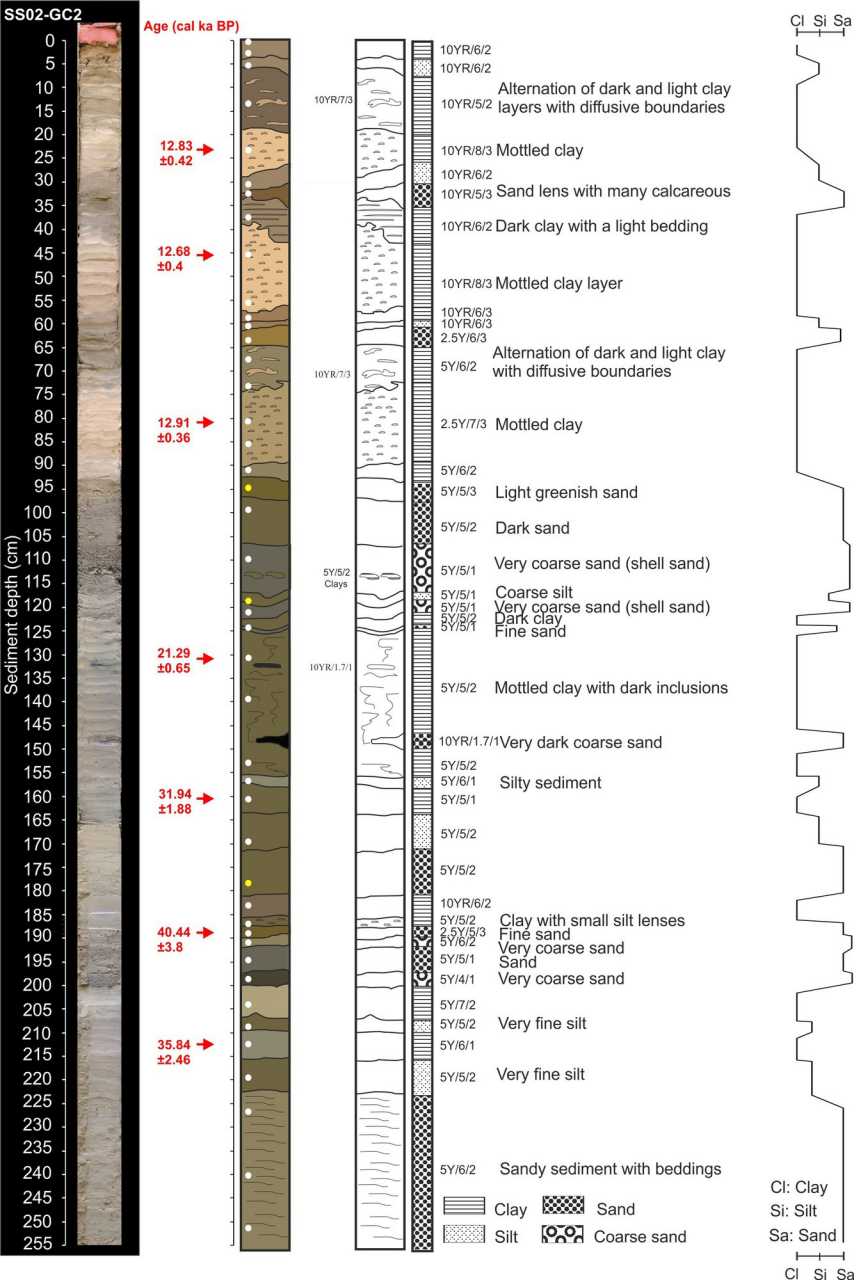
SS02-GC2
Sediment depth (cm)
0
5
10
15
20
25
30
35
40
45
50
55
60
65
70
75
80
85
90
95
100
105
110
115
120
125
130
135
140
145
150
155
160
165
170
175
180
185
190
195
200
205
210
215
220
225
230
235
240
245
250
255
Age (cal ka BP)
12.83 ±0.42
12.68 ±0.4
12.91 ±0.36
21.29 ±0.65
31.94 ±1.88
40.44 ±3.8
35.84 ±2.46
10YR/7/3
10YR/7/3
5Y/5/2 Clays
10YR/1.7/1
10YR/6/2
10YR/6/2
10YR/5/2
Alternation of dark and light clay layers with diffusive boundaries
10YR/8/3
Mottled clay
10YR/6/2
10YR/5/3
Sand lens with many calcareous
10YR/6/2
Dark clay with a light bedding
10YR/8/3
Mottled clay layer
10YR/6/3
10YR/6/3
2.5Y/6/3
5Y/6/2
Alternation of dark and light clay with diffusive boundaries
2.5Y/7/3
Mottled clay
5Y/6/2
5Y/5/3
Light greenish sand
5Y/5/2
Dark sand
5Y/5/1
Very coarse sand (shell sand)
5Y/5/1
Coarse silt
5Y/5/1
Very coarse sand (shell sand)
5Y/5/2
Dark clay
5Y/5/1
Fine sand
5Y/5/2
Mottled clay with dark inclusions
10YR/1.7/1
Very dark coarse sand
5Y/5/2
5Y/6/1
5Y/5/1
Silty sediment
5Y/5/2
5Y/5/2
10YR/6/2
5Y/5/2
Clay with small silt lenses
2.5Y/5/3
Fine sand
5Y/6/2
Very coarse sand
5Y/5/1
Sand
5Y/4/1
Very coarse sand
5Y/7/2
5Y/5/2
Very fine silt
5Y/6/1
5Y/5/2
Very fine silt
5Y/6/2
Sandy sediment with beddings
Clay
Sand
Silt
Coarse sand
Cl
Si
Sa
Cl: Clay
Si: Silt
Sa: Sand
Cl
Si
Sa

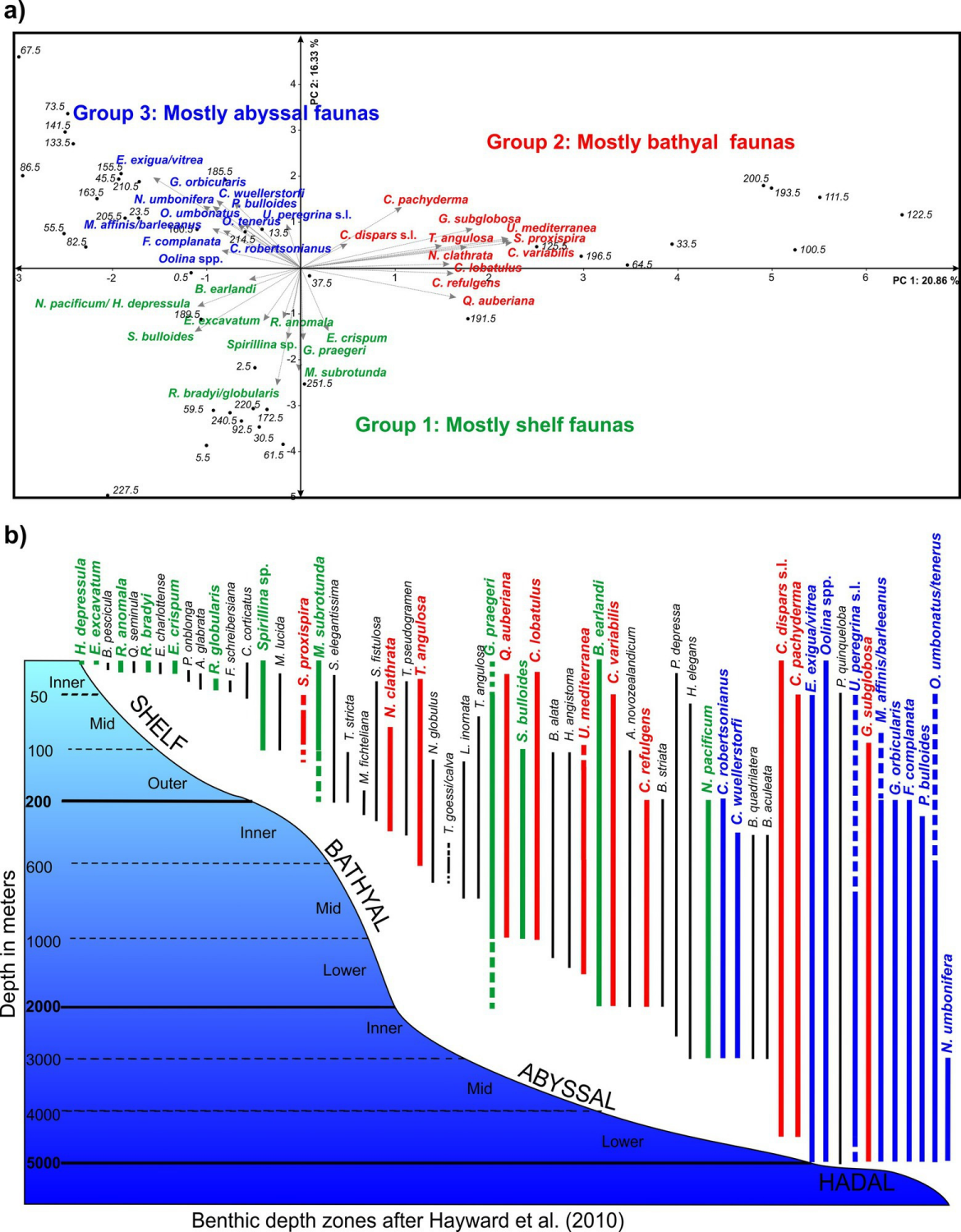

Benthic depth zones after Hayward et al. (2010)

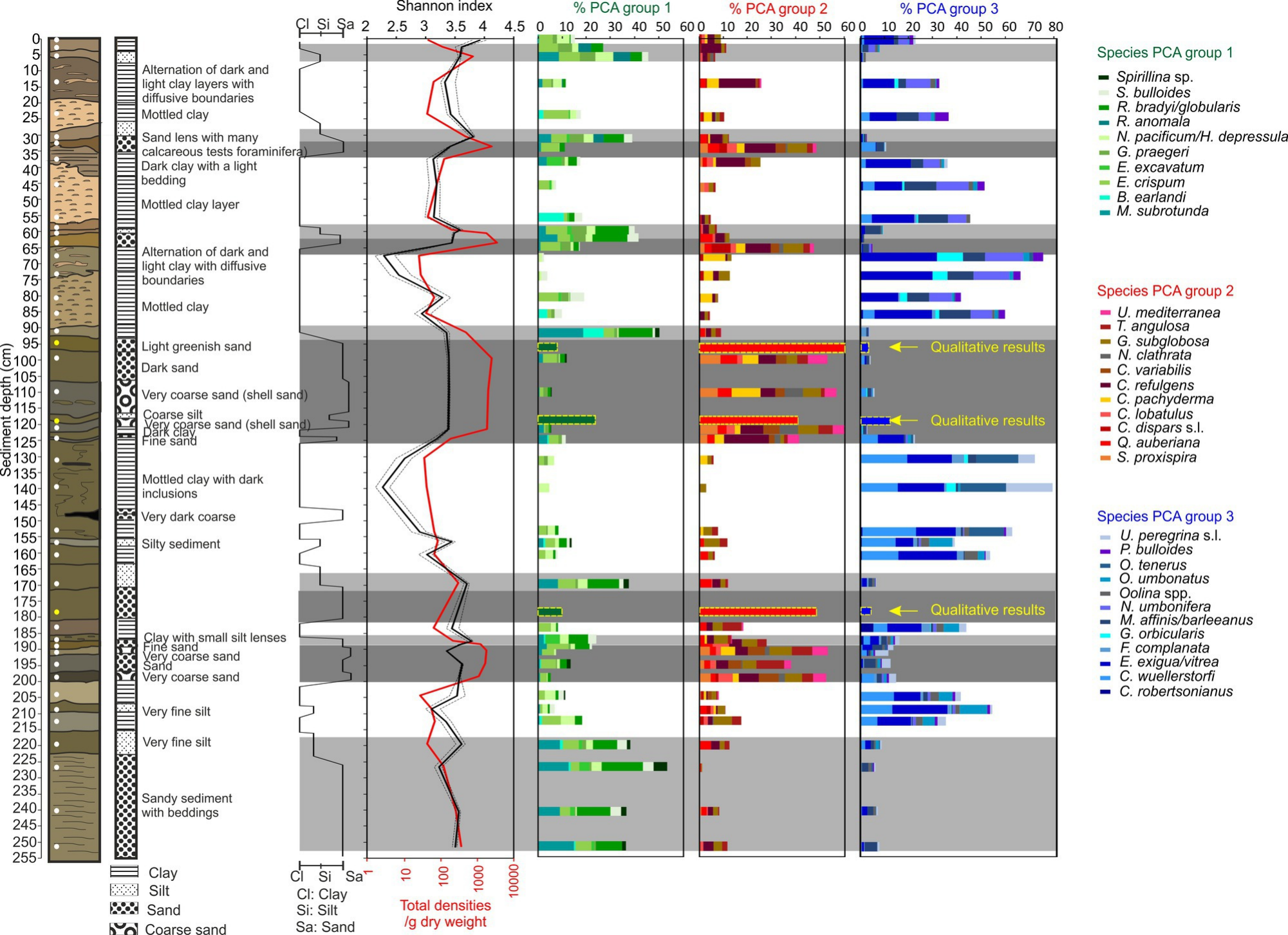
Sediment depth (cm)
Alternation of dark and light clay layers with diffusive boundaries
Mottled clay
Sand lens with many calcareous tests foraminifera)
Dark clay with a light bedding
Mottled clay layer
Alternation of dark and light clay with diffusive boundaries
Mottled clay
Light greenish sand
Dark sand
Very coarse sand (shell sand)
Coarse silt
Very coarse sand (shell sand)
Dark clay
Fine sand
Mottled clay with dark inclusions
Very dark coarse
Silty sediment
Clay with small silt lenses
Fine sand
Very coarse sand
Sand
Very coarse sand
Very fine silt
Very fine silt
Sandy sediment with beddings
Clay
Silt
Sand
Coarse sand
Cl Si Sa
Shannon index
2 2.5 3 3.5 4 4.5
% PCA group 1
% PCA group 2
% PCA group 3
0 10 20 30 40 50 60
0 10 20 30 40 50 60 70 80
Qualitative results
Qualitative results
Qualitative results
Cl Si Sa
1 10 100 1000 10000
Cl: Clay
Si: Silt
Sa: Sand
Total densities /g dry weight
Species PCA group 1
Spirillina sp.
S. bulloides
R. bradyi/globularis
R. anomala
N. pacificum/H. depressula
G. praegeri
E. excavatum
E. crispum
B. earlandi
M. subrotunda
Species PCA group 2
U. mediterranea
T. angulosa
G. subglobosa
N. clathrata
C. variabilis
C. refulgens
C. pachyderma
C. lobatulus
C. dispars s.l.
Q. auberiana
S. proxispira
Species PCA group 3
U. peregrina s.l.
P. bulloides
O. tenerus
O. umbonatus
Oolina spp.
N. umbonifera
M. affinis/barleeanus
G. orbicularis
F. complanata
E. exigua/vitrea
C. wuellerstorfi
C. robertsonianus

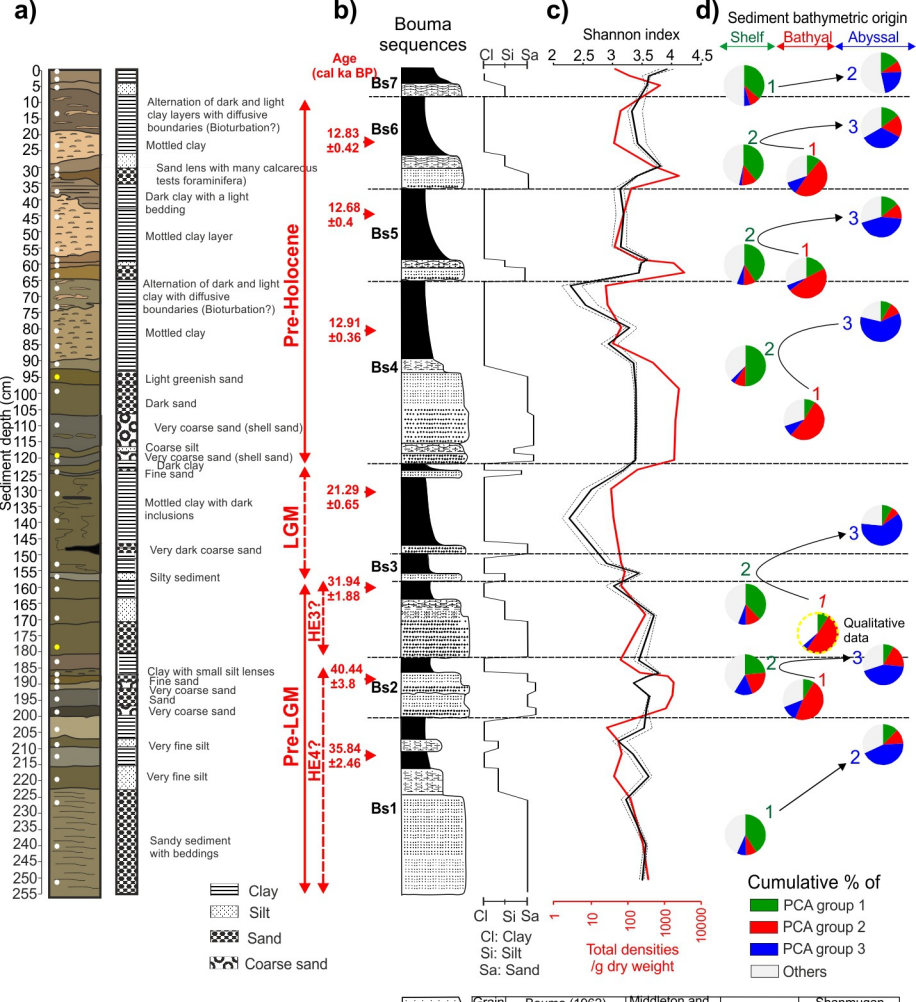

e)

Grain size		Bouma (1962), Divisions	Middleton and Hampton (1973)	Lowe (1982)	Shanmugan (1997)
Mud	T_e	Laminated to homogeneous	Pelagic and low-density turbidity current	Pelagic and hemipelagic	Pelagic and hemipelagic
Sand Silt	T_d	Upper laminae	Turbidity current	Low-density turbidity current	Bottom current reworking
	T_c	Ripples, wavy or contorted laminae			
	T_b	Parallel laminae			
Sand	T_a	Massive graded		High-density turbidity current	Sandy debris flow

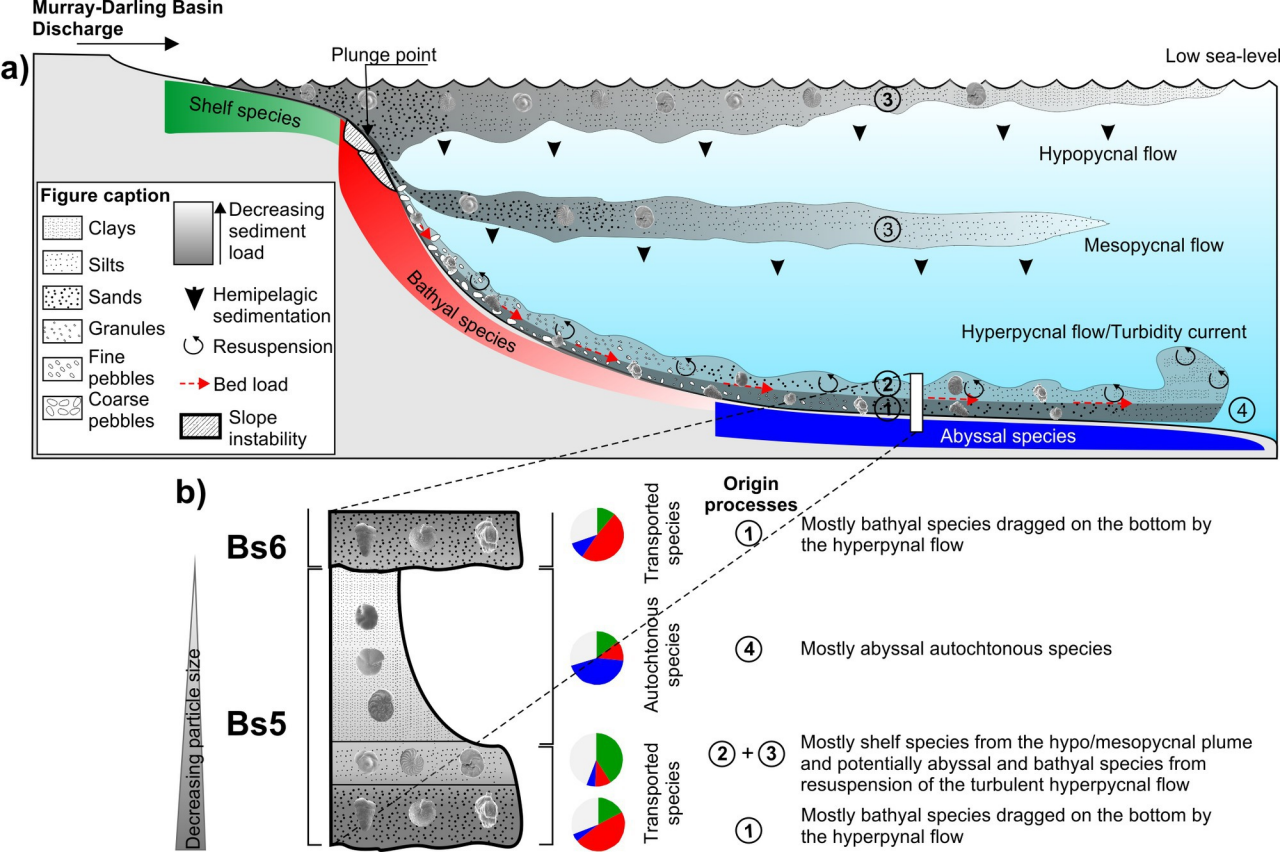
a)
Murray-Darling Basin Discharge
Plunge point
Low sea-level
Shelf species
Bathyal species
Abyssal species
Hypopycnal flow
Mesopycnal flow
Hyperpycnal flow/Turbidity current
Figure caption
Clays
Silts
Sands
Granules
Fine pebbles
Coarse pebbles
Decreasing sediment load
Hemipelagic sedimentation
Resuspension
Bed load
Slope instability
b)
Bs6
Bs5
Decreasing particle size
Transported species
Autochtonous species
Transported species
Origin processes
① Mostly bathyal species dragged on the bottom by the hyperpynal flow
④ Mostly abyssal autochtonous species
② + ③ Mostly shelf species from the hypo/mesopycnal plume and potentially abyssal and bathyal species from resuspension of the turbulent hyperpycnal flow
① Mostly bathyal species dragged on the bottom by the hyperpynal flow

Depth (cm)	Planktonic foraminifera	Uncalibrated ^{14}C age (yr BP)	Error	Average uncalibrated ^{14}C age (yr BP)	Propagated error	Average uncalibrated ^{14}C age after reservoir age correction of 367 ± 167 yrs (yr BP)	Propagated error	Calendar age range(cal yr BP, 2 sigma)		Median calendar age (yr BP)
23	*G. inflata*	11380	90	11335	127	10968	210	13264	12420	12837
23	*O. universa*	11290	90							
45	*G. inflata*	11230	80	11195	120	10828	206	13085	12358	12685
45	*O. universa*	11160	90							
80	*O. universa*	11440	90	11440	90	11073	190	13285	12647	12916
130	*G. inflata*	18020	180	18020	180	17653	246	21911	20633	21291
160	*G. inflata*	28760	670	28225	886	27858	902	33831	30288	31946
160	*O. universa*	27690	580							
188	*G. inflata*	36600	1700	36600	1700	36233	1708	43234	36633	40442
212	Mixed *G. inflata* and *O. universa*	32200	1000	32200	1000	31833	1014	38308	33961	35844